

DETECTION OF GLOBAL POSITIONING SATELLITE ORBIT ERRORS
USING SHORT-BASELINE CARRIER PHASE MEASUREMENTS

BY

FANG-CHENG CHAN

Submitted in partial fulfillment of the
requirements for the degree of
Master of Science in Mechanical and Aerospace Engineering
in the Graduate College of the
Illinois Institute of Technology

Approved _____
Adviser

Chicago, Illinois
July 2001

ACKNOWLEDGEMENT

I would like to thank my advisor, Dr. Boris S. Pervan, for giving me the opportunity and support to pursue this research. His intellectual advice and clear guidance, not only in GPS-based navigation, but also in research and academics, made this thesis possible and benefited my knowledge very greatly. Especially his patient and precious time spent on giving me recommendation while I was working on this thesis. I can't say thanks enough to him. I would also like to thank my defense and reading committees, including Dr. John Way and Dr. Rollin Dix for their valuable advice on this thesis.

I would like to thank all my colleagues, Moon Heo, Irfan Saymi, and Livio Gratton in the Navigation and Guidance Lab for their helpful assistance and advantageous discussion during the time of my research. I would also like to express my appreciation to the Federal Aviation Administration (FAA) for sponsoring my research.

Finally, I would like to thank all my family members and friends for their encouragement and support to my decision of pursuing Master degree after leaving college for ten years. Especially thank my parents, Yi-Ming and Hsiao-Yin Chan, and my elder brothers, Fang-Guan and Fang-Hsin Chan, for their unlimited support both on financial and emotional. I dedicate this thesis to them, my dear family.

TABLE OF CONTENTS

	Page
ACKNOWLEDGMENTS.....	iii
LIST OF TABLES.....	vi
LIST OF FIGURES.....	vii
LIST OF SYMBOLS.....	ix
CHAPTER	
I. INTRODUCTION	1
1.1 GPS Background.....	1
1.2 GPS Satellite Constellation	5
1.3 Differential GPS.....	9
1.4 Orbit Ephemeris Error.....	11
1.5 Prior Work.....	12
II. EFFECT OF ORBIT EMPHEMERIS ERRORS ON DGPS USERS.....	16
2.1 Effective Differential Range Error Across A Given Baseline	16
2.2 The LAAS Precision Approach and Landing System	23
2.3 Impact On Aircraft Precision Approach	28
III. DUAL FREQUENCY MONITOR ARCHITECTURE	38
3.1 Widelane Observable Using Dual Frequency	38
3.2 Estimation of Carrier Cycle Ambiguities.....	40
3.3 Range Measurement Error Requirements	46
3.4 Preliminary Experiment and Results.....	50
IV. SINGLE FREQUENCY APPROACHES TO EPHEMERIS MONITORING.....	55
4.1 Pseudorange Differential Baseline Method	55
4.2 Time History Method by Using L1 Carrier Differential Baseline	56
4.3 Pseudorange Residual Method.....	62
4.4 Carrier-phase Measurement Residual Method.....	66
V. CONCLUSION	70

APPENDIX	72
A. Derivation of Analytic Approach for $\delta\bar{e}_a$	72
BIBLIOGRAPHY	75

LIST OF TABLES

Table	Page
2.1 Accuracy Requirements In LAAS Cat. III.....	26
2.2 Integrity, Continuity, and Availability Requirements in LAAS Cat. III.....	26

LIST OF FIGURES

Figure	Page
1.1 Three Segments in GPS-based Navigation System	2
1.2 GPS-24 Satellite Constellation	6
1.3 General Differential GPS Configuration	10
2.1 Geometry between Satellite and Reference Antennas	17
2.2 Geometry Among Reference Receiver, Satellite and the Earth's Center	20
2.3 Sensitivity Factor of Single Differential Ranging Error	22
2.4 Configuration and Terminology of Precision Landing	24
2.5 Integrity Requirements for Precision Landing	25
2.6 The overview of LAAS System	27
2.7 Configuration During Aircraft Approach/Landing	34
2.8 VPL_e Results for $x_0 = -1km$	35
2.9 VPL_e Results for $x_0 = 0km$	35
2.10 VPL_e Results for $x_0 = 1km$	36
3.1 Probability Multipliers Variations.....	46
3.2 Initialize Waiting Time Intervals	48
3.3 Relations between STD of Measurements and Number of Samples	48
3.4 Relations between STD of Code measurements and Un-correlated	49
3.5 Relative Position of Two Antennas	51
3.6 Residuals of Double Difference Carrier Phase Measurements	52
3.7 Carrier Residuals with Ephemeris Error Injection	53
3.8 Orbital Position Errors due to Ephemeris Error	53

Figure	Page
4.1 VPL_e Results for $x_0 = 0km$ Using Pseudorange Measurements	56
4.2 Worst Case r/s Ratio VS. Time	60
4.3 Simulation Results of P_{eff} Values by Pseudorange Measurements	65
4.4 Simulation Results of P_{eff} Values by Carrier Measurements	67
4.5 Simulation Results of P_{eff} Values by Combination Measurements	68
4.6 P_{eff} Values Performance Improvement by Using 200m Baseline	69

LIST OF SYMBOLS

Symbol	Definition
\bar{e}_a^i	unit line-of-sight vector from antenna 'a' to satellite 'i'
N_a^i	ambiguous integer in carrier phase measurements between antenna 'a' and satellite 'i'
$P()$	probability of some event.
R_a^i	range between reference antenna 'a' to satellite 'i'
\bar{R}_a^i	range vector from reference antenna 'a' to satellite 'i'
\bar{R}_i	position vector of satellite 'i'
\bar{R}_a	position vector of antenna 'a'
\bar{x}_b	baseline vector between reference antennas
$\bar{x}_{a/c}$	baseline vector between reference antenna and aircraft
δ	deviation
$\delta\bar{e}_a^i$	line-of-sight error vector from antenna 'a' to satellite 'i'
$\delta\bar{R}_i$	orbit error vector of satellite 'i'
δt_i	satellite 'i' clock error
δt_a	receiver 'a' clock error
Δ	single difference
Δ^2	double difference
v_ρ	noise of pseudorange raw measurements
v_ϕ	noise of carrier phase raw measurements

Symbol	Definition
ϕ_a^i	carrier phase measurement from antenna 'a' to satellite 'i'
ρ_a^i	pseudorange measurement from antenna 'a' to satellite 'i'
σ_ρ	standard deviation of the noise of pseudorange measurements
σ_ϕ	standard deviation of the noise of carrier phase measureme

CHAPTER I

INTRODUCTION

The Global Positioning System (GPS) was designed in the 1970s primarily to support military uses such as weapon delivery and ship navigation. However, after two decades of system development, it has become an important and versatile utility for civil society. The following section introduces the background and basic working architecture of GPS; more detailed descriptions of related GPS issues are given in subsequent sections. All GPS applications are founded on these basic concepts.

1.1 GPS Background

The current GPS system architecture was proposed by the Department of Defense (DoD) Joint Program Office in 1973 under the direction of Dr. Bradford W. Parkinson. This proposal was a synthesis of all prior satellite navigation systems (such as Transit, Timation and 621B Project) in order to meet requirements of all of the armed services [Parkin94]. By the suggestion of a DoD decision maker, the program was also named “NAVSTAR.” After significant effort in development and tests, initial operational capability was declared at the end of 1993 and full operational capability was attained by the end of 1994.

The whole system consists of three segments [Spilker94c]: the space segment, the control segment and the user segment, as shown in Figure 1.1. The space segment comprises 24 space vehicles (SV) in order to provide a global signal coverage. Each of these satellites continuously transmits a ranging signal that includes navigation data. Element of the broadcast navigation data will be covered in more detail later because of

its close relation to the subject of this research. The control segment consists of five monitor stations (with plans to add more), four ground antenna upload stations, and an Operational Control Center. The main objectives of ground control segment include maintaining each satellite in its proper orbit, keeping satellite clock error within requirements, generating and uploading navigation data to each satellite, and commanding major relocation when a satellite failure occurs. The user segment includes all user receivers. These user receivers track the ranging signal of selected satellites and calculate user positions and local time.

GPS satellites broadcast the ranging signals along with navigation data in two different frequencies: the L1 band, centered at 1575.42 MHz, and the L2 band, centered at 1227.6 MHz. The L1 band signal is modulated with C/A code and P(Y) code in phase quadrature. The L2 band signal is modulated with P(Y) code, (although plans to add

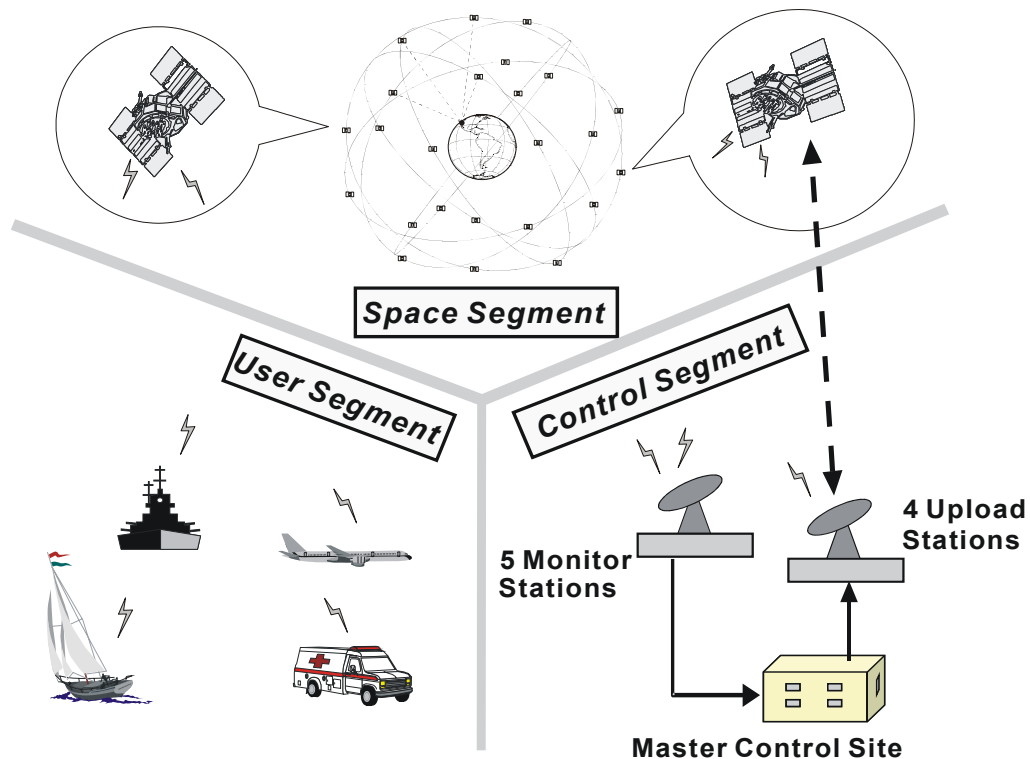


Figure 1.1 Three Segments in GPS-based Navigation System

C/A code modulation to L2 band are presently under development). Civil users can only access C/A code, while the more precise P(Y) codes are accessible only by the military. Both the L1 and L2 frequencies are also modulated with navigation data (50bps) which include satellite orbit ephemerides. The service provided by C/A code is called Standard Position Service (SPS). In similar way, the service provide by P(Y) code is called Precise Position Service (PPS). When a civil user receiver is tracking a satellite signal, it can measure the distance between the receiver and the satellite using a Delay Lock Loop (DLL). We can express this measurement with the following equation:

$$\rho_i = |R_i - R_u| + c \cdot b_u + \varepsilon_{\rho_i} \quad (1-1)$$

where the left side is the C/A code measurement between satellite i and user receiver; the first term in the right side is the distance between the position vector of the i th satellite (R_i) which can be calculated from the broadcast ephemeris and the position vector of user receiver (R_u) receiving it. The second term ($c \cdot b_u$) is the product of the difference between receiver's clock and GPS system time (b_u) and the speed of light (c). This term is a bias common to all satellite measurement. The third term includes measurement error sources such as satellite clock offset from GPS time, tropospheric delay, ionospheric delay, satellite ephemeris error, multipath error, and receiver noise. Since code measurements are the composite of true ranges and other error sources, we use a more suitable name, *pseudorange*, to indicate the raw code measurement of user receiver.

In order to estimate user position, R_u , and receiver clock bias error, $c \cdot b_u$, we linearize the measurement equation about a nominal value - a prior estimate of R_u .

Defining a prior estimate of state vector $\hat{x} = [\hat{R}_u \quad c \cdot \hat{b}_u]^T$ and an estimate of other error sources as $\hat{\varepsilon}_{\rho_i}$, we can predict the pseudorange measurement as follows:

$$\hat{\rho}_i = |R_i - \hat{R}_u| + c \cdot \hat{b}_u + \hat{\varepsilon}_{\rho_i}$$

We define the difference between the actual pseudorange measurement and the prediction of pseudorange as the measurement residual: $\Delta\rho_i = \hat{\rho}_i - \rho_i$. The linearized measurement equation can be written as:

$$\Delta\rho_i = \begin{bmatrix} -\hat{1}_i^T & 1 \end{bmatrix} \begin{bmatrix} \Delta R_u \\ c \cdot \Delta b_u \end{bmatrix} + \Delta\varepsilon_{\rho_i} \quad (1-2)$$

where

$$\hat{1}_i \equiv \frac{R_i - \hat{R}_u}{|R_i - \hat{R}_u|}, \text{ is the estimated line of sight unit vector,}$$

$$\Delta R \equiv \hat{R}_u - R_u, \quad \Delta b_u \equiv \hat{b}_u - b_u, \quad \Delta\varepsilon_i \equiv \hat{\varepsilon}_{\rho_i} - \varepsilon_{\rho_i}$$

Because we have three position states and one clock bias state, we must have four or more satellites in view to resolve the state vector. A matrix equation can express the stack of these four or more measurement residuals equations as follows:

$$\Delta\rho = G\Delta x + \Delta\varepsilon \quad (1-3)$$

$$\text{where } \Delta\rho = \begin{bmatrix} \Delta\rho_1 \\ \Delta\rho_2 \\ \vdots \\ \Delta\rho_n \end{bmatrix}, \quad G = \begin{bmatrix} -\hat{1}_1^T & 1 \\ -\hat{1}_2^T & 1 \\ \vdots & \vdots \\ -\hat{1}_n^T & 1 \end{bmatrix}, \quad \Delta x_i = \begin{bmatrix} \Delta R_u \\ c \cdot \Delta b_u \end{bmatrix}, \quad \text{and } \Delta n = \begin{bmatrix} \Delta\varepsilon_{\rho 1} \\ \Delta\varepsilon_{\rho 2} \\ \vdots \\ \Delta\varepsilon_{\rho n} \end{bmatrix}$$

The pseudorange measurement noise ($\Delta\varepsilon$) is assumed to be zero mean, so the least squares solution to set of normal equations is obtained as follows:

$$\Delta\hat{x} = (G^T G)^{-1} G^T \Delta\rho \quad (1-4)$$

If the measurement error variances are not equal across all satellites, a diagonal weighting matrix $W^{-\frac{1}{2}}$ [Axelrad94, Liu97] may be introduced to give a weighted least squares estimate:

$$\Delta\hat{x} = (G^T W^{-1} G)^{-1} G^T W^{-1} \Delta\rho \quad (1-5)$$

When a prior estimate of user position used to construct matrix G is off by a large amount (a few kilometers), we may iterate until the change of the least squares estimate is sufficiently small. However, matrix G is constructed from line-of-sight unit vectors and the satellite distance from the user is very large, it is not very sensitive to prior position estimate error.

The equations defined above represent the basic single point solution in GPS positioning. In general, more precise pseudorange measurements (small $\Delta\varepsilon_\rho$) and good satellite geometry (well separated and redundant) will result in a more accurate user position estimate.

This paper will focus on one of the error sources in pseudorange measurement: *satellite orbit ephemeris errors*. The effect of ephemeris errors in Differential GPS (DGPS) users, and the limitations of current methods to monitor ephemeris will be explored. Finally, a new superior ephemeris monitor architecture and algorithm will be proposed and shown to be feasible.

1.2 GPS Satellite Constellation

From the last two equations, one can see that the geometry matrix G plays an important role in estimating user position. It is necessary to understand how satellite

geometry effects estimation errors in order to analyze the impact on estimate errors originating from pseudorange measurement errors.

The operational satellite constellation [Spilker94b] consists of 24 satellites in six orbit planes with four satellites in each orbit plane. Figure 1.2 shows this constellation. Each orbit plane is inclined 55° with respect to the equatorial plane and with nodes

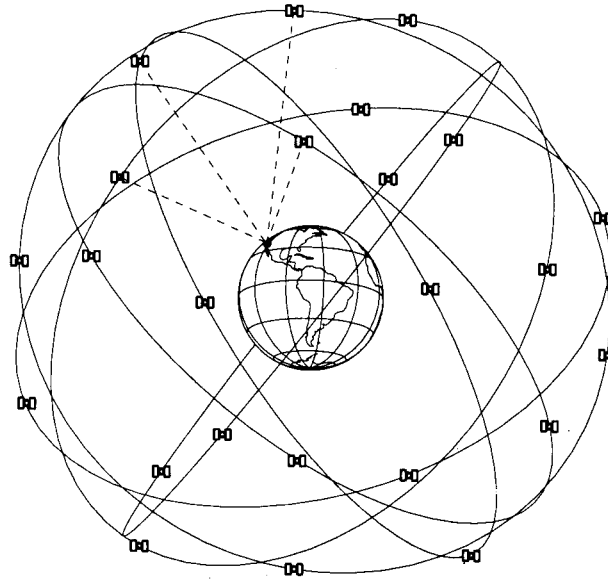


Figure 1.2 GPS-24 Satellite Constellation

separated in longitude by 60° from the adjacent plane. The semi-major axis of every satellite orbit is nominally 26,561.75 km, with a period of 12 hours. The reason for choosing inclined orbits instead of equatorial orbits is that satellites in equatorial orbits can not be viewed by the user at a latitude higher than 72° (in current GPS satellite altitude). The period of 12 hours sidereal time is chosen not only because of repeatable satellite ground tracks, but also due to the possible use of carrier phase/Doppler measurements. The requirement for a minimum of four satellites in view with good geometry leads to the current multiple satellite constellation.

All parameters of the GPS satellite constellation were designed to meet the objective of providing global GPS ranging signal coverage at any time. In the nominal GPS constellation, there are always at least five satellites in view for an elevation angle above 5°. If the mask elevation angle is 10°, the vicinity of 35° to 55° latitude will have a minimum of four satellites in view for a short period each day. In these areas, the possibility of the number of satellites in view falling below the minimum requirement of four does exist when a satellite outage occurs. The mean anomaly of each satellite in the GPS-24 constellation was designed to minimize the impact of such a satellite outage.

From equations (1-4) and (1-5), it can be seen how the satellite geometry affects position estimate error. For the unweighted case (Equation (1-4)), the Geometric Dilution of Precision (GDOP) is defined to quantify the impact of satellite geometry on estimate errors as follows:

$$GDOP = \frac{1}{\sigma} \sqrt{\sigma_x^2 + \sigma_y^2 + \sigma_z^2 + \sigma_b^2} \quad (1-6)$$

where σ is standard deviation of pseudorange measurement noise and σ_x , σ_y , σ_z , and σ_b are the corresponding standard deviations of position errors in the x , y , z directions and the receiver clock error, respectively.

Since $\Delta x = [\Delta X \quad \Delta Y \quad \Delta Z \quad \Delta b]^T$, the value under the square root of equation (1-6) is equal to $tr[E(\Delta x \Delta x^T)] = tr[\text{cov}(\Delta x)]$. By using the Equation (1-4), $\text{cov}(\Delta x)$ can be computed as follows:

$$\begin{aligned} \text{cov}(\Delta \hat{x}) &= E[(G^T G)^{-1} G^T \Delta \rho \Delta \rho^T G (G^T G)^{-1}] \\ &= (G^T G)^{-1} G^T E(\Delta \rho \Delta \rho^T) G (G^T G)^{-1} \\ &= (G^T G)^{-1} G^T \text{cov}(\Delta \rho) G (G^T G)^{-1} \end{aligned} \quad (1-7)$$

Assuming all of the measurement noises are independent, zero mean, and of equal variance σ^2 , one can obtain following results:

$$\text{cov}(\Delta\rho) = I\sigma^2, \text{ and } \text{cov}(\Delta\hat{x}) = (G^T G)^{-1} \sigma^2 \quad (1-8)$$

where I is the identity matrix. By using Equations (1-6) and (1-8), GDOP can be expressed as follows:

$$GDOP = \frac{1}{\sigma} \sqrt{\text{tr}[\text{cov}(x)]} = \sqrt{\text{tr}[(G^T G)^{-1}]} \quad (1-9)$$

In the same manner, we can also define other DOP factors similar to GDOP:

$$PDOP = \frac{1}{\sigma} \sqrt{\sigma_x^2 + \sigma_y^2 + \sigma_z^2} \dots \text{Position Dilution of Precision.}$$

$$HDOP = \frac{1}{\sigma} \sqrt{\sigma_x^2 + \sigma_y^2} \dots \text{Horizontal Dilution of Precision.}$$

$$VDOP = \frac{\sigma_z}{\sigma} \dots \text{Vertical Dilution of Precision.}$$

$$TDOP = \frac{\sigma_b}{\sigma} \dots \text{Time Dilution of Precision.}$$

All these DOP factors can be easily computed once the result of $(G^T G)^{-1}$ is obtained.

The assumption of independent pseudorange measurement noise with equal variance on all satellites is not always true, especially for low elevation angle satellites. For satellites at low elevation angles, residual tropospheric and ionospheric errors and multipath errors sometimes become larger and correlative. In this case, a “weighted” DOP may be derived from Equation (1-5). But for the present purposes, namely understanding the impact of satellite geometry on estimate errors, the independent, and identically distributed error assumption is sufficient and will make upcoming derivations more clear.

1.3 Differential GPS

The horizontal accuracy of Standard Position Service (SPS) users is about 100m (95 percentile level) when Selective Availability (SA) - an intentional degradation of the ranging signal induced by the DoD - is activated. In order to improve the accuracy and integrity of SPS, the differential GPS (DGPS) technique [Parkin95] was proposed and developed. The concept of DGPS exploits the correlation of ranging errors between the reference station and DGPS user receivers to effectively eliminate co-existing ranging errors in user ranging measurement. Today, DGPS techniques are very common in many applications that need precise positioning. This technique can improve SPS navigation accuracy to be better than 1m (one sigma). Although SA has been inactivated now, the User Equivalent Ranging Error (UERE) is still at the five meter level, when multiplied by PDOP value – normally is two or three - the positioning error will be at the 10 to 20 meter level. This is not good enough for applications requiring meter-level accuracy, such as aircraft precision landing. The precision landing scenario is explored in detail in this paper.

Figure 1.3 shows a typical DGPS architecture. Usually DGPS applications require a high quality GPS receiver in a surveyed location as a reference station. This reference station estimates the slowly varying measurement errors and forms a correction for each satellite in view. The correction is broadcasted to all DGPS users within an operational service radius of the reference station. This differential correction greatly improves accuracy for all DGPS users within the service range, regardless of whether SA is active or not.

However, there are some limitations to DGPS. The basic idea of DGPS is that

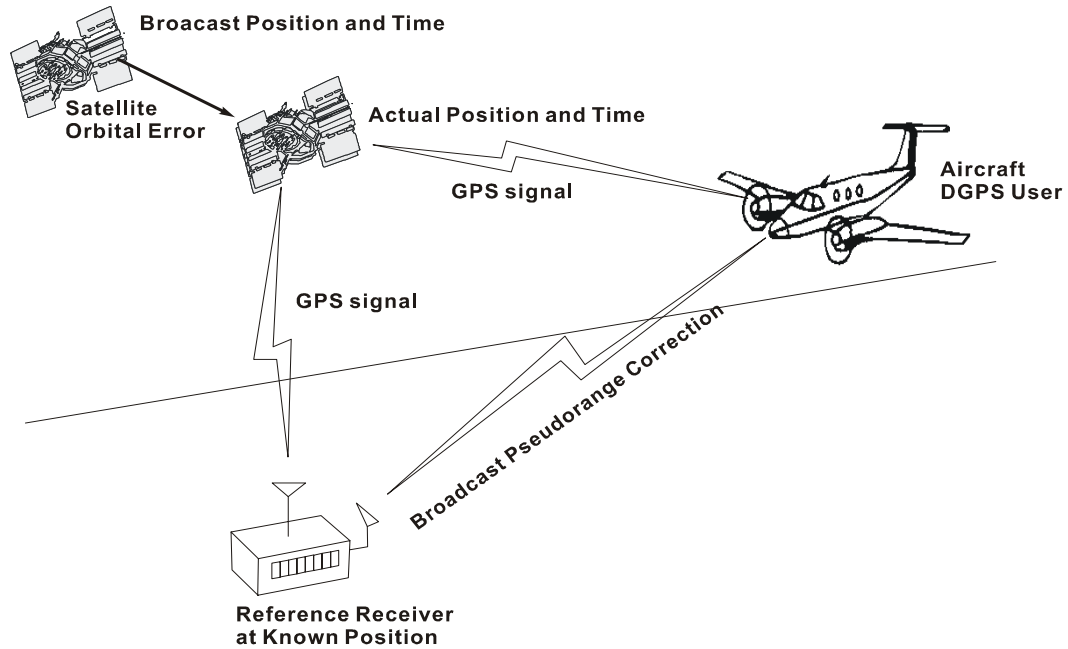


Figure 1.3 General Differential GPS Configuration

ranging corrections can eliminate common ranging errors between the user and the reference station. Because ranging corrections formed by the reference station are geographically separated from the user and delayed in application, these corrections are not the exact corrections for users' ranging errors. The differences between ranging corrections and user ranging errors are called differential ranging errors. There are three types of differential ranging errors:

1. *Decorrelation with Distance*: Ranging errors between reference station and users that are caused by geographical separation (such as ionospheric and tropospheric errors and ephemeris errors).
2. *Decorrelation with Time*: Ranging errors between reference station and users that are caused by time rate change of the correction. This effect is also called *latency*.
3. *Uncorrelated Errors*: The errors are not common between reference station

and users. Errors of this type are not correctable with DGPS (e.g. receiver noise and multipath errors).

Any DGPS application should be carefully designed to mitigate the effects of such differential ranging errors.

The Local Area Augmentation System (LAAS) is an aircraft precision landing system developed by Federal Aviation Administration (FAA) with the objective to replace current Instrument Landing System (ILS). The LAAS architecture is based on the DGPS concept [MASPS98], and will serve as the baseline DGPS architecture considered in this work.

1.4 Orbit Ephemeris Error

Whenever the broadcast GPS navigation message does not contain the correct satellite orbit parameters, an ephemeris error is said to exist. There are a number of potential causes of such errors: Master Control Station (MCS) uploads erroneous data, navigation data transmit errors from the satellite, scheduled or unscheduled satellite maneuvering, etc. Fortunately, all ephemeris errors can be categorized into just two classes:

Class A Failures: The ephemeris data is incorrect after the satellite performs an *unscheduled* maneuver from its nominal orbit. The probability of such a failure is relatively small because multiple safeguards exist on GPS satellites to prevent the uncommanded firing of satellite thrusters. Yet this scenario did happen [Rivers00]; fortunately, because only the small attitude thrusters aboard the spacecraft were involved, the resulting orbit error was negligible.

Class B Failures: The current broadcast ephemeris does not represent the actual satellite orbit (but no unscheduled satellite maneuvers are involved).

These two failure classes differ in that archived ephemeris data (i.e., an earlier, validated ephemeris broadcast) can be used to detect class B failures, whereas class A failures can only be detected by measurements. These ideas will be discussed in detail later in this work.

In most typical (non-failure) situations, the radial component (in the direction from center of earth to the satellite) of orbit error is smaller than the tangential and cross-track components. For stand-alone users (non-DGPS), only the errors projected into line-of-sight directions matter. These projected ephemeris errors directly contribute to pseudorange measurement error. According to a report [Bowen86] during phase one in 1984, “for predictions of up to 24 hours, the rms ranging error attributable to ephemeris was 2.1m”. In contrast, the position accuracy of DGPS users is influenced by ephemeris errors orthogonal to line-of-sight unit vectors. In addition, the error introduced into differential correction increases as the distance between the reference station and the user increases. It will be shown in the next chapter that the error grows linearly with separation between user and reference station.

1.5 Prior Work

To date, only a small amount of research effort has been focused on monitoring ephemeris anomalies. In the LAAS ground facility, the consistency of new and old ephemeris messages is checked [PT1LAAS], but as noted earlier, such monitoring has no capability to detect Class A failures. Receiver Autonomous Integrity Monitor (RAIM) is another approach to detect many different types of failures in a relatively simple way.

An alternative algorithm (DPR/DPDAS), proposed by Shuichi Matsumoto, et al [Matsu97], can detect three dimensional orbit errors when another healthy satellite is available. These algorithms are introduced briefly here:

Built-in LAAS Ephemeris Monitoring. In Category I LAAS ground systems, a standard set of monitoring procedures have been defined. These standard procedures can be roughly categorized into three steps [Matsu97]:

Step one – LAAS Ground Facility (LGF) receivers automatically confirm that the navigation messages of each satellite meet all requirements of the GPS SPS Interface Control Document (ICD) [ICD-200]. This includes checking that satellite health bits and other health-related bits all indicate that message data is good.

Step two – Ephemeris/ephemeris check. Normally ephemeris changeovers occur every two hours because predicted orbit curves are optimized for a two-hour period. After each changeover, the LGF compares satellite locations given by the old ephemeris and the new ephemeris to make sure that these two ephemeris messages are consistent. A checking standard of 250m is set on the three-dimension satellite position difference.

Step three – Each broadcasted pseudorange correction and correction rate will be checked by LGF to confirm that they lie within $\pm 327.6\text{m}$ and $\pm 3.4\text{m/s}$, respectively. These limits represent not-to-exceed (NTE) values for correction size.

These procedures are suitable to manage ephemeris integrity risk for a certain class of ephemeris failures given that a good prior ephemeris exists. When no good prior ephemeris data exists, such as after a satellite maneuver, these tests are insufficient.

Receiver Autonomous Integrity Monitor (RAIM). The RAIM concept [Brown92], [Parking88], [Sturza88] is based on the verification the consistency of redundant satellites measurements by the GPS user (the aircraft in our case). RAIM is an advantageous approach to fault detection because it can detect many different types of failures in a relatively simple way. The performance of RAIM is limited, however, by the need for redundant satellites (more than the minimum of four required for positioning). In general, the quality of RAIM performance is a strong function of the number of satellites in view and the specific satellite line-of-sight geometries. Furthermore, for aircraft navigation with LAAS, it is a system requirement that both space and ground segment failures must be detected and isolated by the LGF before differential corrections are broadcast. The aircraft is accountable only for the management of failures in its own navigation avionics. For this reason, RAIM is not a viable candidate for LAAS ephemeris monitoring. (RAIM must be implemented at the aircraft to detect failures in the space and ground segments.)

DPR / DPDAS Method. An algorithm has been proposed by Shuichi Matsumoto, et al. [Matsu97] to detect three-dimensional orbit error. This algorithm uses the Differential Pseudorange Residual method (DPR) to detect orbit error parallel to the LGR-satellite line-of-sight direction, and the Double Phase Difference with Ambiguity Search method (DPDAS) to detect orbit error perpendicular to the line-of-sight direction. The advantages of these two methods are that they are executed on the ground and only need one other (already-approved) GPS satellite in view to verify whether another new satellite ephemeris is good enough or not. The disadvantage of the DPR algorithm is that the orbit error it detects has almost no influence on LAAS DGPS users. The DPDAS

algorithm is effective, but only when carrier phase cycle ambiguities can be correctly identified. However, the ambiguity search technique proposed in this regard is not sufficiently reliable. In addition, algorithm performance was not quantified relative to LAAS integrity requirements.

Because aircraft precision landing application requires a DGPS architecture with both high accuracy and integrity, ephemeris monitoring is an important issue here. The objective of this paper is to propose a more effective and integral method of monitoring ephemeris error to protect LAAS users from any hazardous satellite orbit error (both class A and B failures) in real time. The effect of ephemeris error on DGPS users is fully examined in the next chapter, and a *Vertical Protection Level (VPL)* bound is defined.

In order to meet the requirements of LAAS and provide real-time warning capability, a dual frequency ephemeris monitoring architecture is proposed in Chapter III, and a preliminary experiment based on collected measurement data is performed. It is shown that the dual frequency monitor architecture can fulfill the intentioned objective with realizable LGF hardware.

In Chapter IV, a few single frequency ephemeris monitoring methods are discussed and their performance is evaluated. Although the performance of the dual frequency algorithm is shown to be sufficient for all types of ephemeris failures, we will show a certain classes of ephemeris failures (Type B) can also be detected by single frequency methods.

CHAPTER II

EFFECT OF ORBIT EMPHEMERIS ERRORS ON DGPS USERS

In Section 1.4, it was stated that the effect of ephemeris errors in DGPS applications will grow as the distance between the reference station and the user increases. In this chapter, a detailed quantitative discussion is presented, and the impact on a LAAS category III user (aircraft) will be fully explored.

2.1 Effective Differential Range Error Across A Given Baseline

Consider a baseline vector, \bar{x}_b , between two GPS receivers aligned due east (to simplify error analysis without lost generality). L1 band carrier-phase measurements between satellite i and receivers a , and b can be expressed as:

$$\lambda_1 \phi_a^i = R_a^i + c \cdot (\delta t_i - \delta t_a) - I_i + T_i + \lambda_1 N_a^i + \nu_\phi \quad (2-1)$$

$$\lambda_1 \phi_b^i = R_b^i + c \cdot (\delta t_i - \delta t_b) - I_i + T_i + \lambda_1 N_b^i + \nu_\phi \quad (2-2)$$

where λ_1 is the wavelength (m) of L1 carrier signal; ϕ_a^i is the carrier-phase measurement of receiver a to satellite i ; R_a^i is true range between satellite i and the reference receiver a ; c is the constant of light speed; δt_i and δt_a are the corresponding satellite i and receiver a clock errors with respect to GPS time; I_i is the ionospheric delay of the radio signal of satellite i (minus sign here signifies phase advance); T_i is the tropospheric delay of the radio signal of satellite i ; N_a^i is the unknown integer cycle ambiguity of carrier-phase measurement between satellite i and receiver a ; ν_ϕ is the measurement error due to receiver noise and multipath. All these definitions are also applicable to the carrier-

phase measurement of receiver b by replacing a with b . We assume \bar{x}_b is short enough that ionosphere and troposphere errors are the same for the two receivers.

The single difference carrier-phase measurement can be obtained by subtracting equation (2-2) from equation (2-1). The result is equation (2-3):

$$\lambda_1 \Delta \phi_{ab}^i = \Delta R_{ab}^i + c \cdot (\delta t_b - \delta t_a) + \lambda_1 \Delta N_{ab}^i + \Delta v_\phi \quad (2-3)$$

where $\Delta \phi_{ab}^i \equiv \phi_a^i - \phi_b^i$, $\Delta R_{ab}^i \equiv R_a^i - R_b^i$, $\Delta N_{ab}^i \equiv N_a^i - N_b^i$

In Figure 2.1, the line-of-sight unit vectors, \bar{e}_a and \bar{e}_b , can be treated as parallel because

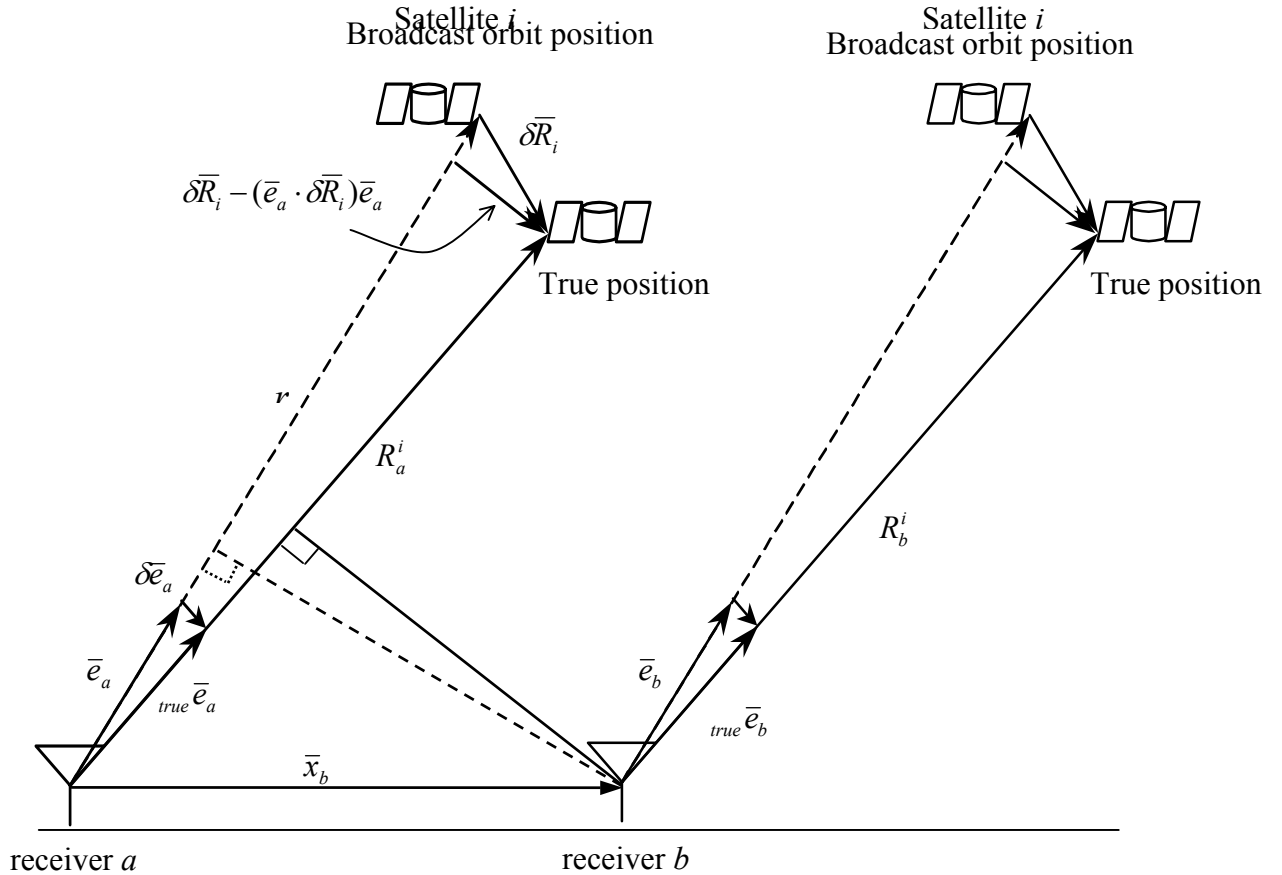


Figure 2.1 Geometry between Satellite and Reference Antennas

the ranges between satellite and receivers (over 20000 km) are much larger than the distance between two receivers (which we limit to a few kilometers maximum). The single difference of true ranges can be found from Figure 2.1 as:

$$\Delta R_{ab}^i = R_a^i - R_b^i =_{true} \bar{e}_a \cdot \bar{x}_b = (\bar{e}_a + \delta\bar{e}_a) \cdot \bar{x}_b = \bar{e}_a \cdot \bar{x}_b + \delta\bar{e}_a \cdot \bar{x}_b \quad (2-4)$$

The inner product $\bar{e}_a \cdot \bar{x}_b$ is the difference of “nominal” ranges between receiver a and receiver b obtained using the broadcast ephemeris of satellite i . The second term, $\delta\bar{e}_a \cdot \bar{x}_b$, represents the effective differential ranging error due to the error in knowledge of satellite position.

We define this differential ranging error for satellite i as:

$$\delta\Delta\phi_i \equiv \Delta R_{ab}^i - \bar{e}_a \cdot \bar{x}_b = \delta\bar{e}_a \cdot \bar{x}_b \quad (2-5)$$

The line-of-sight unit vector error $\delta\bar{e}_a$ can be derived from two different approaches to achieve the same result:

1. Geometry approach: (from Figure 2.1 directly)

$$\begin{aligned} \delta\bar{e}_a &= \frac{|\delta\bar{R}_i - (\delta\bar{R}_i \cdot \bar{e}_a)\bar{e}_a|}{R_a^i} \times \frac{[\delta\bar{R}_i - (\delta\bar{R}_i \cdot \bar{e}_a)\bar{e}_a]}{|\delta\bar{R}_i - (\delta\bar{R}_i \cdot \bar{e}_a)\bar{e}_a|} = \frac{[\delta\bar{R}_i - (\delta\bar{R}_i \cdot \bar{e}_a)\bar{e}_a]}{R_a^i} \\ &= \frac{\delta\bar{R}_i - (\delta\bar{R}_i^T \bar{e}_a)\bar{e}_a}{R_a^i} = \frac{\bar{I} - (\bar{e}_a \bar{e}_a^T)}{R_a^i} \delta\bar{R}_i \end{aligned} \quad (2-6)$$

We can replace the true range R_a^i by nominal range r plus projection of orbit error on to a nominal line-of-sight unit vector :

$$R_a^i = r + \delta\bar{R}_i \cdot \bar{e}_a$$

Substituting this equation into (2-6) and dropping second and higher order terms in

$\delta\bar{R}_i$ gives:

$$\delta\bar{e}_a = \frac{1}{r} (\bar{I} - \bar{e}_a \bar{e}_a^T) \delta\bar{R}_i \quad (2-6.1)$$

2. Analytic approach: (see Appendix A)

Substituting Equation (2-6.1) into Equation (2-5), we can express differential ranging error directly as a function of satellite orbit error ($\delta\bar{R}_i$) and the baseline vector \bar{x}_b between receivers:

$$\delta\Delta\phi_i = \delta\bar{e}_a \cdot \bar{x}_b = \frac{1}{r} [(\bar{I} - \bar{e}_a \bar{e}_a^T) \delta\bar{R}_i]^T \bar{x}_b = \frac{[\delta\bar{R}_i - (\delta\bar{R}_i^T \bar{e}_a) \bar{e}_a]^T \bar{x}_b}{r}$$

It could be useful if we had some idea of how these variables interact with each other. Since orbit error is arbitrary, we can normalize the bound of single differential ranging error with respect to the scale of the baseline vector. Consider now a satellite whose line-of-sight vector is defined by azimuth angle ψ and elevation angle θ , in east-north-up coordinates, can be represented as:

$$\bar{e}_a = \cos \theta \cos \psi \hat{i}_1 + \cos \theta \sin \psi \hat{i}_2 + \sin \theta \hat{i}_3 \quad (2-7)$$

The baseline vector (due east) with length b is $\bar{x}_b = [b \ 0 \ 0]^T$. Substituting this baseline vector into Equation (2-6.2) to get the result of single differential ranging error, one obtains:

$$\begin{aligned} \delta\Delta\phi_i &= \delta\bar{e}_a^T \bar{x}_b \\ &= \frac{1}{r} \begin{bmatrix} \delta x & \delta y & \delta z \end{bmatrix} \begin{bmatrix} (1 - \bar{e}_{ax} \bar{e}_{ax}) & -\bar{e}_{ax} \bar{e}_{ay} & -\bar{e}_{ax} \bar{e}_{az} \\ -\bar{e}_{ay} \bar{e}_{ax} & (1 - \bar{e}_{ay} \bar{e}_{ay}) & -\bar{e}_{ay} \bar{e}_{az} \\ -\bar{e}_{az} \bar{e}_{ax} & -\bar{e}_{az} \bar{e}_{ay} & (1 - \bar{e}_{az} \bar{e}_{az}) \end{bmatrix} \begin{bmatrix} b \\ 0 \\ 0 \end{bmatrix} \end{aligned}$$

where \bar{e}_{ax} , \bar{e}_{ay} , and \bar{e}_{az} are the east, north, and up components of \bar{e}_a as defined in Equation (2-7). Therefore, we have:

$$\delta\Delta\phi_i = \frac{1}{r} \begin{bmatrix} \delta x & \delta y & \delta z \end{bmatrix} \begin{bmatrix} (1 - \bar{e}_{ax} \bar{e}_{ax}) & -\bar{e}_{ay} \bar{e}_{ax} & -\bar{e}_{az} \bar{e}_{ax} \end{bmatrix}^T b$$

Dividing through by length b (scalar) and substituting Equation (2-7) into the above, the normalized single differential ranging error becomes:

$$\frac{\delta\Delta\phi_i}{b} = \frac{1}{R_a^i} [(1 - \cos^2\theta \cos^2\psi) \quad -\cos^2\theta \sin\psi \cos\psi \quad -\cos\theta \sin\theta \cos\psi]^T \begin{bmatrix} \delta x \\ \delta y \\ \delta z \end{bmatrix} \quad (2-8)$$

Figure 2.2 shows the geometry relationship among the Earth's center, the receiver antenna, the satellite range r , the Earth's radius R_E , and the radius of satellite orbit R_S .

Using the law of cosines, the range r can be expressed by R_E , R_S , elevation angle and

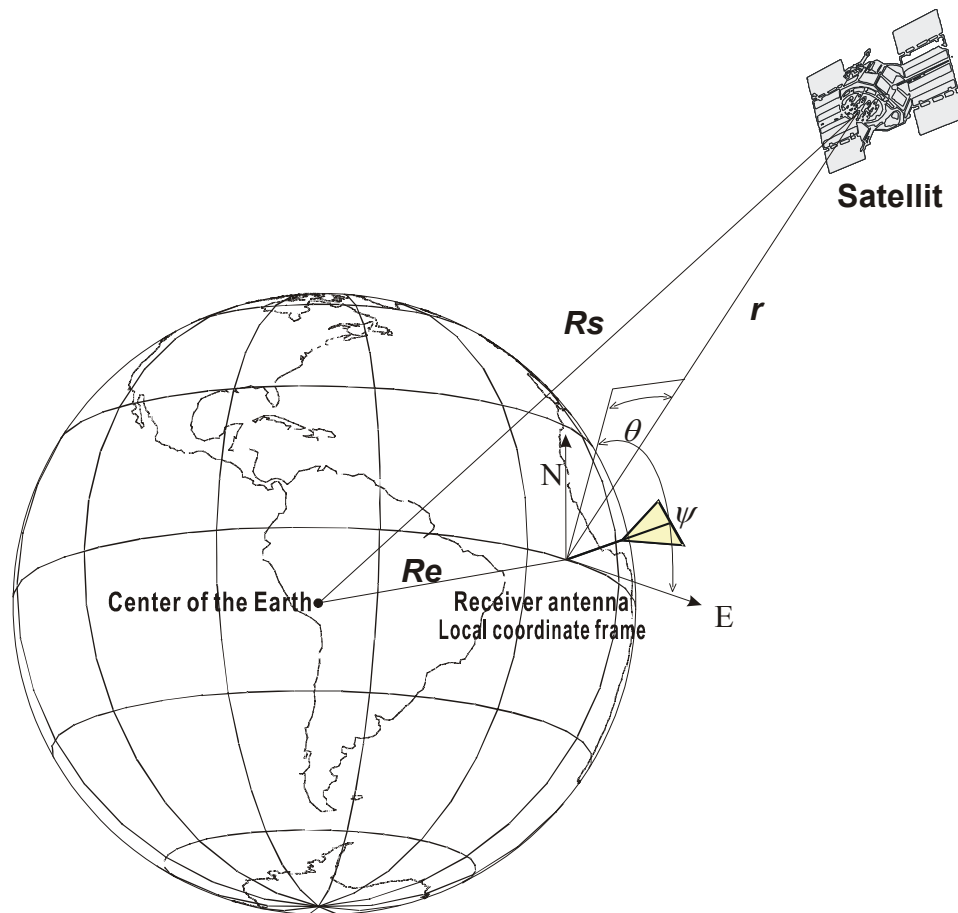


Figure 2.2 Geometry Among Reference Receiver, Satellite and the Earth's Center

azimuth angle:

$$R_s = R_E + r - 2rR_E \cos\left(\frac{\pi}{2} + \theta\right)$$

Solving for r :

$$r = R_E \left(\sqrt{\frac{R_s^2}{R_E^2} - \cos^2 \theta} - \sin \theta \right) \quad (2-9)$$

Substituting Equation (2-9) into Equation (2-8), the relation between normalized single differential ranging error and satellite orbit error can be shown as:

$$\frac{\delta \Delta \phi_i}{b} = F(\theta, \psi)^T \delta R_i \quad (2-10)$$

where $F(\theta, \psi)^T$ is equal to:

$$\frac{1}{R_E} \left[\begin{array}{ccc} \frac{1 - \cos^2 \theta \cos^2 \psi}{\left(\sqrt{\frac{R_s^2}{R_E^2} - \cos^2 \theta} - \sin \theta \right)} & \frac{-\cos^2 \theta \sin \psi \cos \psi}{\left(\sqrt{\frac{R_s^2}{R_E^2} - \cos^2 \theta} - \sin \theta \right)} & \frac{-\cos \theta \sin \theta \cos \psi}{\left(\sqrt{\frac{R_s^2}{R_E^2} - \cos^2 \theta} - \sin \theta \right)} \end{array} \right]$$

By the Schwarz inequality, the normalized bounded single differential ranging error can be obtained as follows:

$$\left\| \frac{\delta \Delta \phi_i}{b} \right\| \leq \|F(\theta, \psi)\| \|\delta R_i\| \quad (2-11)$$

$\|F(\theta, \psi)\|$ represents the worst case sensitivity to orbit error displacement $\|\delta R_i\|$. Figure 2.3 is a three dimensional polar plot of $\|F(\theta, \psi)\|$ (worst-case sensitivity values) corresponding to different satellite elevation angle (θ) and azimuth angle (ψ). The elevation angles vary from 0 to 90° and azimuth angles vary from 0 to 360° . In Figure 2.3, the Z coordinate is equal to $\|F(\theta, \psi)\|$.

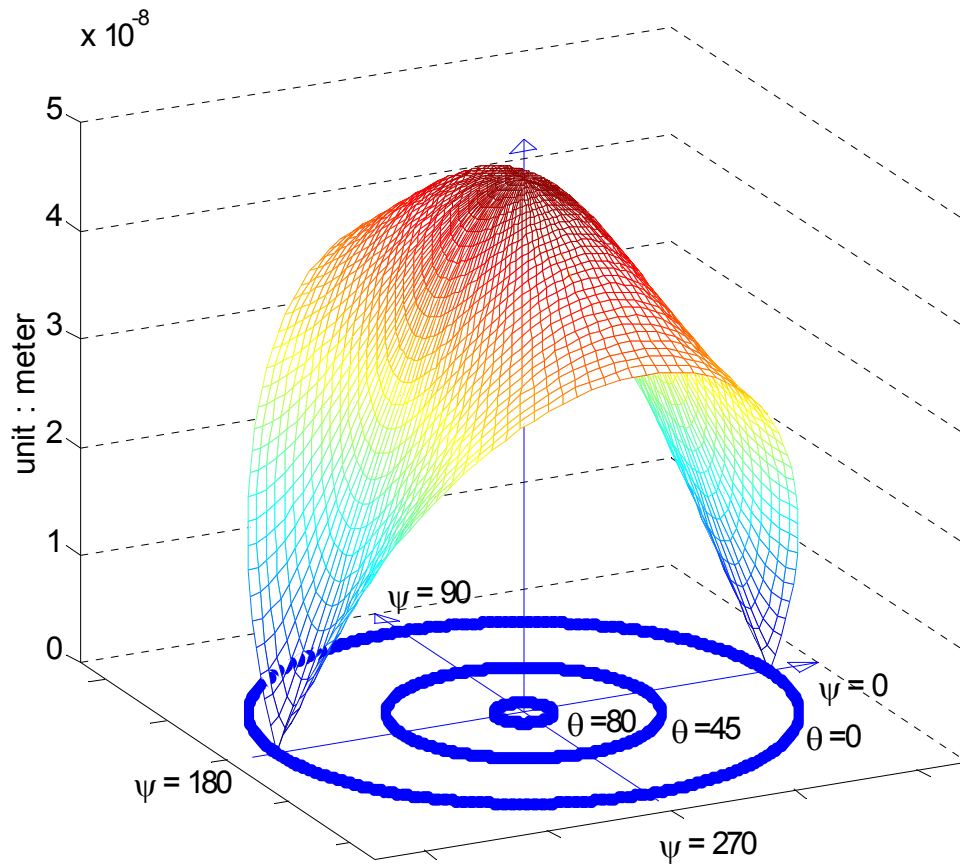


Figure 2.3 Sensitivity Factor of Single Differential Ranging Error

It is evident from the figure that only zero elevation satellites with azimuths at 0° or 180° will experience zero effective ranging error due to orbit error. In all other cases, an effective ranging error will generally exist; the largest magnitudes occurring for high elevation satellites.

2.2 The LAAS Precision Approach and Landing System

In this work, we are particularly interested in the impact of orbit errors on DGPS navigation for aircraft precision landing. In this regard, a brief review of the relevant navigation requirements is necessary. The DGPS system being developed under the direction of Federal Aviation Administration (FAA) is known as the Local Area Augmentation System (LAAS). The navigation performance requirements for the system are rated according to a three-tiered structure (Category I, II, and III). A Category III facility will support automatic precision landing operation and has the most stringent requirements. In this work, we assume a Category III system.

Figure 2.4 shows the configuration for an aircraft precision approach/landing and graphical definitions of some related terminology:

RDP: Runway Datum Point.

GPIP: Glide Path Intercept Point.

DCH (DH): Datum Crossing Height.

FPAP: Flight Path Alignment Point.

Glidepath Angle: standard approach angle (3° normally).

WGS-84 Ellipsoid: A model of Earth's actual physical shape [WGS84].

H: Height above RDP of aircraft position translated onto the final approach path (Table 2.1).

D: Horizontal distance above of aircraft position from the RDP translated along the final approach path (Table 2.1).

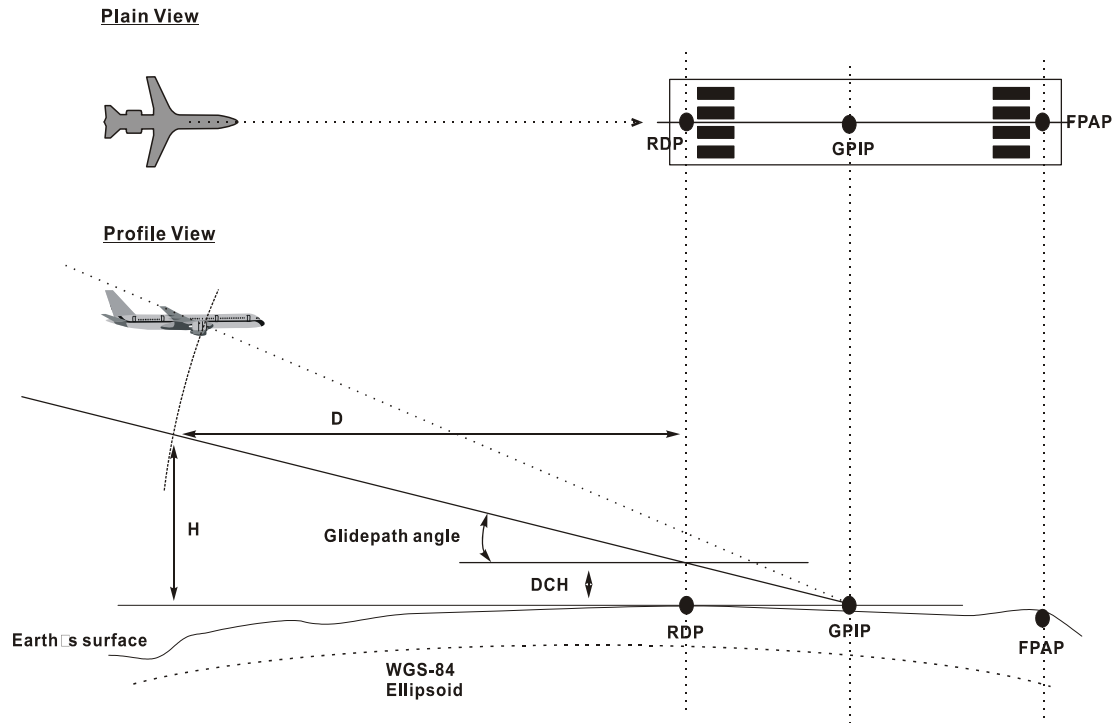


Figure 2.4 Configuration and Terminology of Precision Landing

Allocation of specific requirements of the navigation system is based on four fundamental parameters [Davis93, ORD95]:

Accuracy. Accuracy is the measure of the navigation output deviation from truth under fault-free conditions, often specified in terms of 95% performance.

Integrity. Integrity is the ability of a system to provide timely warnings to users when the system should not be used for navigation. *Integrity risk* is the probability of an undetected navigation error or failure that results in hazardously misleading information onboard the aircraft.

Continuity. Continuity is the likelihood that the navigation signal-in-space supports accuracy and integrity requirements for the duration of intended operation. *Continuity risk* is the probability of a detected but unscheduled navigation function interruption after an approach has been initiated.

Availability. Availability is the fraction of time the navigation function is usable (as determined by its compliance with the accuracy, integrity, and continuity requirements) before the approach is initiated.

Because the focus here is on applications in Cat. III, we only list the requirements of Performance Type III of LAAS [MASPS98] in Table 2.1 and Table 2.2. Table 2.1 lists the vertical accuracy requirements. Because the vertical *Navigation System Error (NSE)* limit is more stringent than lateral *NSE* limit, our focus will be on meeting the vertical requirements only.

The *Vertical Alert Limit (VAL)* is defined as 2.5 times the 95% vertical *NSE* limit [MASPS98]. Figure 2.5 is a plot of the *VAL* versus aircraft height for Cat. III. The unit of height is “feet” but the unit of *VAL* value is “meter” (in order to be consistent with system specifications).

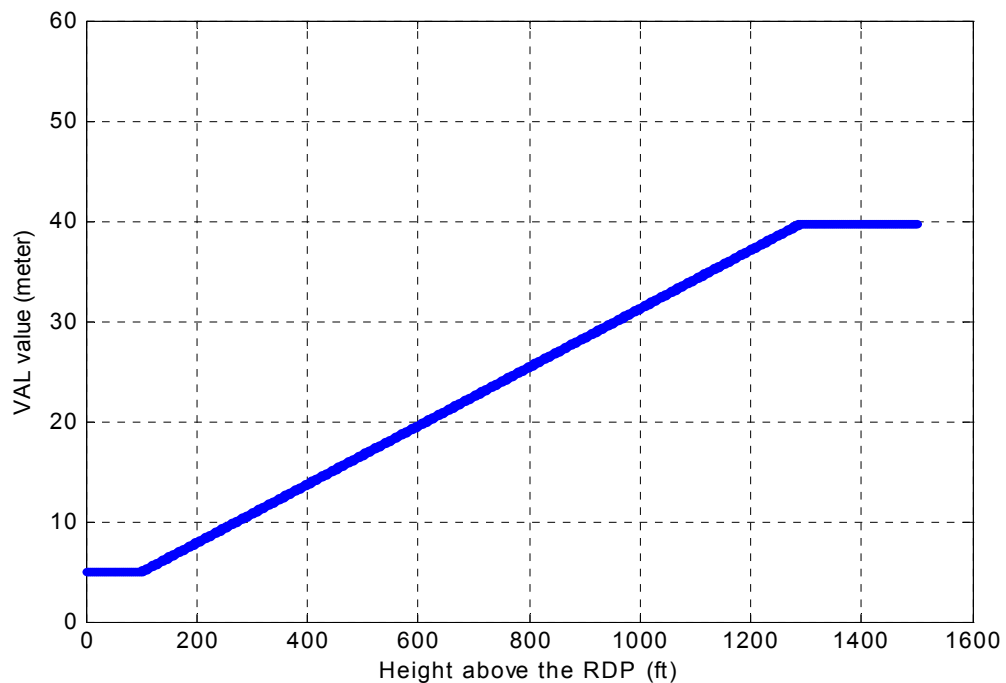


Figure 2.5 Integrity Requirements for Precision Landing

Table 2.1 Accuracy Requirements In LAAS Cat. III

95% Vertical <i>NSE</i> Limit (meters)	Height (H) above RDP of aircraft position translated onto the final approach path (feet)	95% Lateral <i>NSE</i> Limit (meters)	Horizontal distance (D) of aircraft position from the RDP as translated along the final approach path (meters)
≤ 2.0	$H \leq 100$	≤ 6.2	Beyond RDP and along runway
$\leq 0.0117 * H(\text{ft}) + 0.83$	$100 < H \leq 1290$	$\leq 0.000704 * D(\text{m}) + 6.2$	$0 < D \leq 7212$
≤ 15.9	$H > 1290$	≤ 11.3	$H > 7212$

Table 2.2 Integrity, Continuity, and Availability Requirements in LAAS Cat. III

Allowable Integrity Risk	Allowable Continuity Risk	Availability
1×10^{-9} per approach	lateral : 2×10^{-6} / 30 seconds vertical : 2×10^{-6} / 15 seconds	0.99 to 0.99999

The *VAL* represents an integrity containment surface in the sense that the probability of an undetected vertical position error exceeding the *VAL* must be less than 1×10^{-9} (the integrity risk requirement in Table 2.2). This integrity requirement applies for both fault-free and faulted (e.g. orbit error) case.

The LAAS is a application of DGPS. The most relevant difference of the LAAS reference station from others in DGPS applications is the existence of multiple receivers. Figure 2.6 shows the overview of LAAS system. The LAAS Ground Facility (LGF) uses multiple receivers separated by baseline to collect ranging signals from all satellites in view, computes the ranging correction and correction rate for each ranging signal, and then broadcasts these corrections and correction rates twice per second to LAAS users (aircraft).

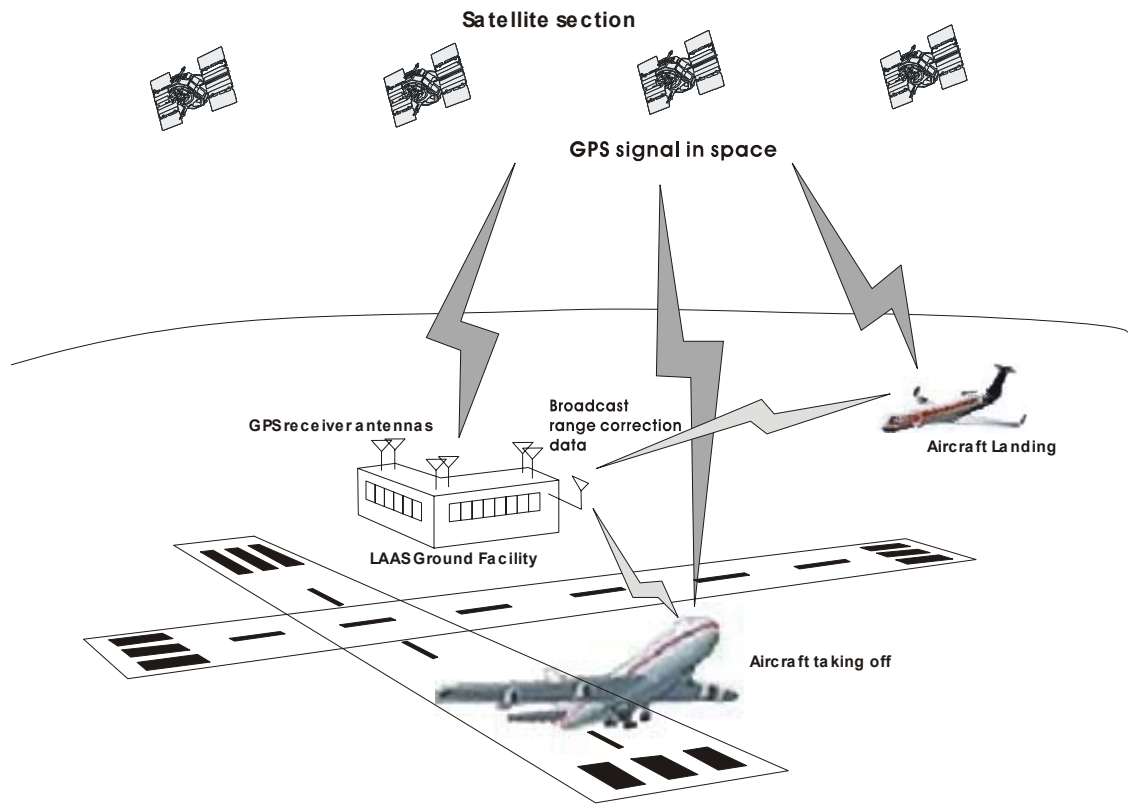


Figure 2.6 The overview of LAAS System

The benefits of the implementation of multiple receivers are improving accuracy of ground range measurements by averaging results of each receiver and providing a means for detection and isolation of failed reference receiver.

In this work, we will investigate the effectiveness of using carrier-phase measurements across the LAAS reference receiver baselines to detect orbit ephemeris errors to ensure navigation integrity.

2.3 Impact On Aircraft Precision Approach

The objective of integrity monitoring in LAAS ground stations is to ensure the probability of *Hazardous Misleading Information (HMI)* provided by pseudorange corrections from the ground station is sufficiently small. For example when the *NSE* exceeds the *VAL* without annunciation within the time to alarm, an *HMI* event is said to have occurred. Unfortunately, *true* user position is unknown, the actual *NSE* can not be determined. Instead, a statistical upper bound on position error can be found by using satellite geometry and known measurement error statistics. This upper bound position error, in the vertical direction, is called the *Vertical Protection Level (VPL)*, and likewise, in lateral direction, is known as *Lateral Protection Level (LPL)*.

Thus to ensure integrity in case of an ephemeris failure, a *VPL* value under ephemeris failure hypothesis must be calculated and compared with *VAL*. In this work, assume the maximum number of satellites with ephemeris failures at any time is one. The ephemeris messages for each satellite are created and broadcast independently. The likelihood of multiple simultaneous ephemeris failures is assumed to be negligible. Using Equation (2-10), the pseudorange single difference between reference station and aircraft ranging error for the failed satellite can be shown to be:

$$\delta\Delta\rho_f = (F_f^T \delta R_f) x_{a/c} + \Delta v_{\rho_f} \quad (2-12)$$

where subscript indication f indicates the index of the failed satellite; $x_{a/c}$ is a scalar range between the phase center of reference receivers and that of aircraft receiver; Δv_{ρ_f} is single difference of measurement noise in this failed satellite. In this case, the vector F_f is defined via projection along of the direction of displacement $x_{a/c}$ rather than due east as assumed earlier. Recall that F_f will be a function of the azimuth and elevation of satellite f . For the other healthy satellites, the pseudorange single differential ranging error is:

$$\delta\Delta\rho_i = \Delta v_{\rho_i} \quad (2-13)$$

The measurement error (Δv_{ρ_i}) for each satellite is assumed to be independent and identically normally distributed with zero mean and standard deviation σ_ρ for pseudorange raw measurements and σ_ϕ for carrier-phase raw measurements.

Assume now that we have available a single difference carrier-phase measurement ($\Delta\phi_f$), with cycle ambiguity known and removed, from two ground based reference receivers aligned in the approach path direction. In this case, for the failed satellite we have using (2-10):

$$\frac{\delta\Delta\phi_f - \Delta v_{\phi_f}}{b} = F_f \delta R_f$$

Substituting this equation into (2-12), the pseudorange single differential ranging error can be expressed as:

$$\delta\Delta\rho_f = \left(\frac{\delta\Delta\phi_f - \Delta v_{\phi_f}}{b} \right) x_{a/c} + \Delta v_{\rho_f} \quad (2-14)$$

Now, equation (1-5) can be used to define aircraft position estimate error as a function of the ranging measurement errors as follows:

$$\Delta \hat{x} = S \begin{bmatrix} \delta \Delta \rho_1 \\ \vdots \\ \delta \Delta \rho_f \\ \vdots \\ \delta \Delta \rho_n \end{bmatrix}, \text{ where } S = (G^T G)^{-1} G^T = \begin{bmatrix} s_{11} & s_{12} & \cdots & s_{1n} \\ s_{21} & s_{22} & \cdots & s_{2n} \\ \vdots & \vdots & \ddots & \vdots \\ s_{n1} & s_{n2} & \cdots & s_{nn} \end{bmatrix}$$

In expanded form, this is equivalent to:

$$\Delta \hat{x} = \begin{bmatrix} \delta \hat{x}_{a/c} \\ \delta \hat{y}_{a/c} \\ \delta \hat{z}_{a/c} \\ c \delta \hat{b}_{a/c} \end{bmatrix} = \begin{bmatrix} s_{11} & s_{12} & \cdots & s_{1n} \\ s_{21} & s_{22} & \cdots & s_{2n} \\ \vdots & \vdots & \ddots & \vdots \\ s_{n1} & s_{n2} & \cdots & s_{nn} \end{bmatrix} \begin{bmatrix} \delta \Delta \rho_1 \\ \vdots \\ \delta \Delta \rho_f \\ \vdots \\ \delta \Delta \rho_n \end{bmatrix}$$

$$\Rightarrow \delta \hat{z}_{a/c} = s_{31} \delta \Delta \rho_1 + s_{32} \delta \Delta \rho_2 + \cdots + s_{3f} \delta \Delta \rho_f + \cdots + s_{3n} \delta \Delta \rho_n \quad (2-15)$$

Substituting (2-14) and (2-15) into (2-16):

$$\begin{aligned} \delta \hat{z}_{a/c} &= s_{3f} [(\delta \Delta \phi_f - \Delta v_\phi) \frac{x_{a/c}}{b}] + s_{3f} \Delta v_{\rho_f} + \sum_{\substack{i=1 \\ i \neq f}}^n s_{3i} \Delta v_{\rho_i} \\ &= s_{3f} \frac{x_{a/c}}{b} \delta \Delta \phi_f - s_{3f} \frac{x_{a/c}}{b} \Delta v_\phi + \sum_{i=1}^n s_{3i} \Delta v_{\rho_i} \end{aligned} \quad (2-16)$$

Meanwhile on the ground station, a threshold T_s may be set to test $\delta \Delta \phi$ (which is measurable) in a manner that the false alarm probability is not greater than a certain predetermined value P_{fa} . The basic concept is that if $|\delta \Delta \phi_i|$ exceeds T_s for a given satellite i , then an orbit error has been detected. A probability multiplier K_{ffde} associated with this P_{fa} is defined so that:

$$T_s \equiv K_{ffde} \times \sigma_{\Delta \phi}$$

where $\sigma_{\Delta\phi}$ is the standard deviation of single differential carrier-phase measurement noise. With this detection algorithm in place on the ground, it is always true that:

$$|\delta\Delta\phi_f| < K_{ffde} \times \sigma_{\Delta\phi} \quad (2-17)$$

An inequality equation for vertical position error can then be obtained by a conservative coefficient replacement and substituting (2-17) into (2-16):

$$|\delta z_{a/c}| \leq \|s_{3,:}\|_{\infty} \frac{x_{a/c}}{b} K_{ffde} \sigma_{\Delta\phi} + \left\| \|s_{3,:}\|_{\infty} \frac{x_{a/c}}{b} \Delta v_{\phi} + \sum_{i=1}^n s_{3i} \Delta v_{\rho} \right\| \quad (2-18)$$

where $\|s_{3,:}\|_{\infty}$ is the absolute value of the largest element of $s_{3,:}$ (the infinity norm). Note that the last two terms (within the absolute value) in equation (2-18) are functions of random measurement errors. Invoking our assumption of independent and identically normally distributed measurement error, the standard deviation of the sum of last two terms in equation (2-18) can be conservatively expressed as:

$$\begin{aligned} \sigma\left(\|s_{3,:}\|_{\infty} \frac{x_{a/c}}{b} \Delta v_{\phi} + \sum_{i=1}^n s_{3i} \Delta v_{\rho}\right) &= \sqrt{\|s_{3,:}\|_{\infty}^2 \left(\frac{x_{a/c}}{b}\right)^2 \sigma_{\Delta\phi}^2 + \|s_{3,:}\|_2^2 \sigma_{\Delta\rho}^2} \\ &\leq \|s_{3,:}\|_2 \sqrt{\left(\frac{x_{a/c}}{b}\right)^2 \sigma_{\Delta\phi}^2 + \sigma_{\Delta\rho}^2} \end{aligned} \quad (2-19)$$

Now we define the Vertical Protection Level under the Ephemeris failure hypothesis (VPL_e) based on a desired probability P_{mde} of missed detection for ephemeris error. We introduce a second probability multiplier K_{mde} associated with P_{mde} and define P_{mde} as the upper bound of vertical error using (2-18), (2-19), and the fact that

$$\|s_{3,:}\|_2 > \|s_{3,:}\|_{\infty} :$$

$$|\delta z_{a/c}| \leq VPL_e \equiv \|s_{3,:}\|_2 \left[K_{ffde} \left(\frac{x_{a/c}}{b}\right) \sigma_{\Delta\phi} + K_{mde} \sqrt{\left(\frac{x_{a/c}}{b}\right)^2 \sigma_{\Delta\phi}^2 + \sigma_{\Delta\rho}^2} \right] \quad (2-20)$$

The only satellite geometry dependent parameter in equation (2-20) is s_{3i} , which we would like to eliminate to obtain a generally applicable result. We do this by using existing features of the LAAS architecture which will limit the worst case satellite geometries that can be used under normal conditions. Specifically, assuming the failure free (“ H_0 ”) hypothesis [MASPS98], satellite geometries are always checked to ensure that:

$$VPL_{H_0} \equiv K_{ff_md} \sqrt{\sum_{i=1}^n s_{3i}^2 \sigma_i^2} < VAL$$

where K_{ff_md} is probability multiplier corresponding to the maximum permissible integrity risk ($<10^{-9}$) under the fault free hypothesis. Each σ_i will just be the standard deviation of single differential pseudorange measurement noise $v_{\Delta\rho_i}$; for our case: $\sigma_i = \sigma_{\Delta\rho}$. Using this result and substituting into the above equation, VPL_{H_0} can be obtained as:

$$VPL_{H_0} = K_{ff_md} \sqrt{\sum_{i=1}^n s_{3i}^2 \sigma_{\Delta\rho}^2}$$

During aircraft approach and landing, the satellite geometry almost remains in the same configuration. In order to operate aircraft approach and landing under safe environments, VPL_{H_0} value must not be larger than VAL at any time. The most stringent value of VAL is at the Datum Cross Height (DCH or DH), so VPL_{H_0} should be smaller than VAL_{DH} in the normal operational condition:

$$VAL_{DH} \geq VPL_{H_0} = K_{ff_md} \sqrt{\sum_{i=1}^n s_{3i}^2 \sigma_{\Delta\rho}^2} = K_{ff_md} \sigma_{\Delta\rho} \|s_{3i}\|_2$$

Therefore, the maximum permissible value of $\|s_{3,:}\|_2$ in aircraft approach/landing can be found as:

$$\|s_{3,:}\|_2 \leq \frac{VAL_{DH}}{K_{ff_md} \sigma_{\Delta\rho}} \quad (2-21)$$

where $VAL_{DH} = 5$ m (Performance Type 3) and $K_{ff_md} = 6.673$ (C₄ class)[MASPS98].

Substituting Equation (2-21) into (2-20), we now have:

$$VPL_e \leq VAL_{DH} \left[\frac{K_{ffde}}{K_{ff_md}} \left(\frac{x_{a/c}}{b} \right) \frac{\sigma_{\Delta\phi}}{\sigma_{\Delta\rho}} + \frac{K_{mde}}{K_{ff_md}} \sqrt{\left(\frac{x_{a/c}}{b} \right)^2 \frac{\sigma_{\Delta\phi}^2}{\sigma_{\Delta\rho}^2} + 1} \right] \quad (2-22)$$

Here we define two new coefficients to simplify equation (2-22):

$$K_1 = \frac{K_{ffde}}{K_{ff_md}}, K_2 = \frac{K_{mde}}{K_{ff_md}} \quad (2-23)$$

The simplified equation (2-22) follows:

$$VPL_e \leq VAL_{DH} \left[K_1 \left(\frac{x_{a/c}}{b} \right) \frac{\sigma_{\Delta\phi}}{\sigma_{\Delta\rho}} + K_2 \sqrt{\left(\frac{x_{a/c}}{b} \right)^2 \frac{\sigma_{\Delta\phi}^2}{\sigma_{\Delta\rho}^2} + 1} \right] \quad (2-24)$$

Performance estimation, To evaluate VPL_e , it is necessary to make a few reasonable assumptions about the values of the parameters in equation (2-23):

$\sigma_{\Delta\phi} / \sigma_{\Delta\rho} = 0.05$, assuming the standard deviation of carrier-phase measurement is 1 cm and that of pseudorange measurement is 20 cm (this is a conservatively large ratio) [Misra99].

$$K_{ffde} = 5.33, \quad P_{ffde} \approx 1 \times 10^{-7} \text{ (driven by continuity requirement) [Shively01].}$$

$$K_{mde} = 5.03, \quad P_{mde} \approx 4.99 \times 10^{-7} \text{ [Shively01].}$$

The final probability multiplier is already specified as a LAAS requirement [MASPS98]:

$$K_{ff_md} = 6.673$$

In Figure 2.7, we decompose $x_{a/c}$ into x_0 plus x_{GPIP} , where x_0 is the distance from *GPIP* to the centroid of reference receivers; and x_{GPIP} is the horizontal distance from *GPIP* to the aircraft. Both x_0 and x_{GPIP} are positive in the directions shown in this figure. In order to easily compare VPL_e with VAL , a translated VAL formula set is used. In this formula set, all units are meters and the x coordinate is now the horizontal distance from *GPIP* to aircraft:

$$VAL = \begin{cases} 5m; & x < 581.6m \\ 0.005 \times x + 2.075m; & 581.6m \leq x \leq 7502.6m \\ 39.588m; & x > 7502.6m \end{cases}$$

The following graphs, Figure 2.8, 2.9, and 2.10, show the evaluated results of VPL_e corresponding to different values of x_0 and baseline spans (different b values). The VAL limit is also shown on each graph so that one can easily check if VPL_e performance is good enough or not. The increment of baseline span is 100m in all graphs.

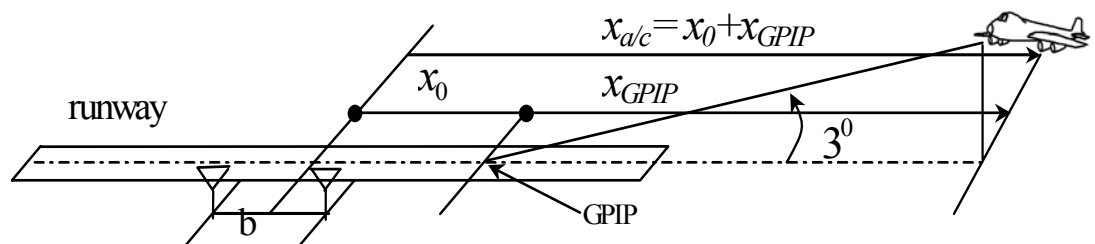
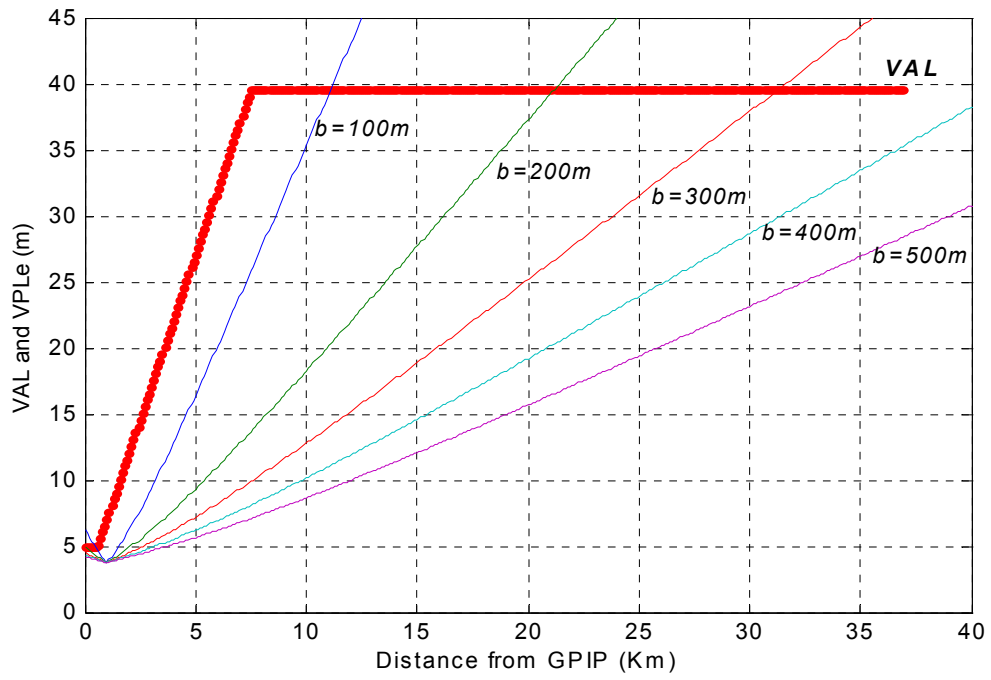
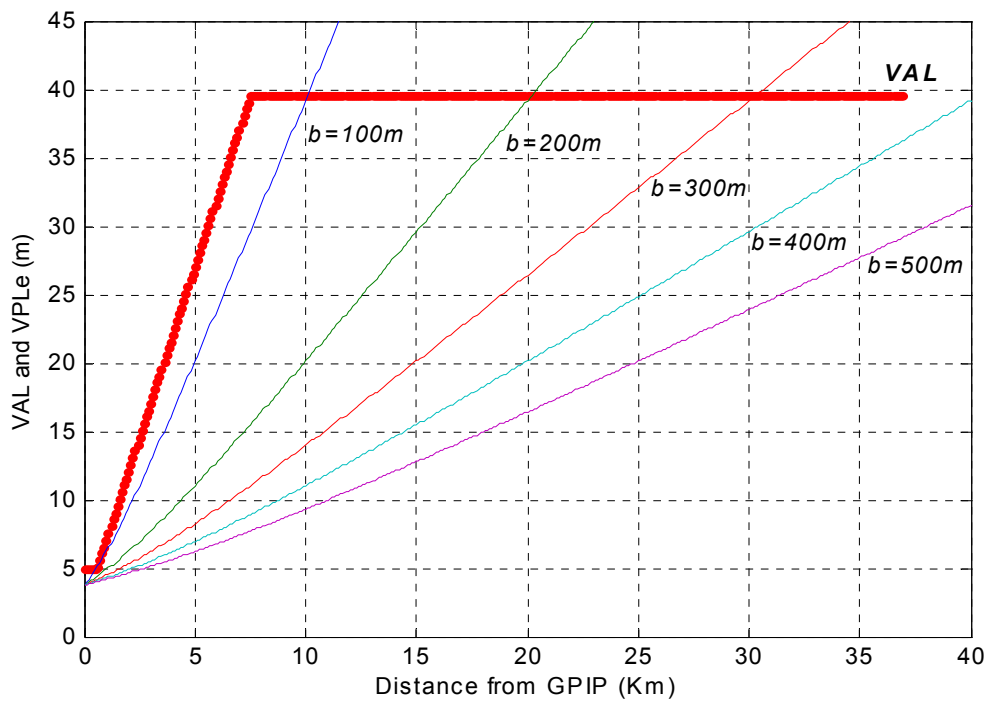


Figure 2.7 Configuration During Aircraft Approach/Landing

Figure 2.8 VPL_e Results for $x_0 = -1km$ Figure 2.9 VPL_e Results for $x_0 = 0km$

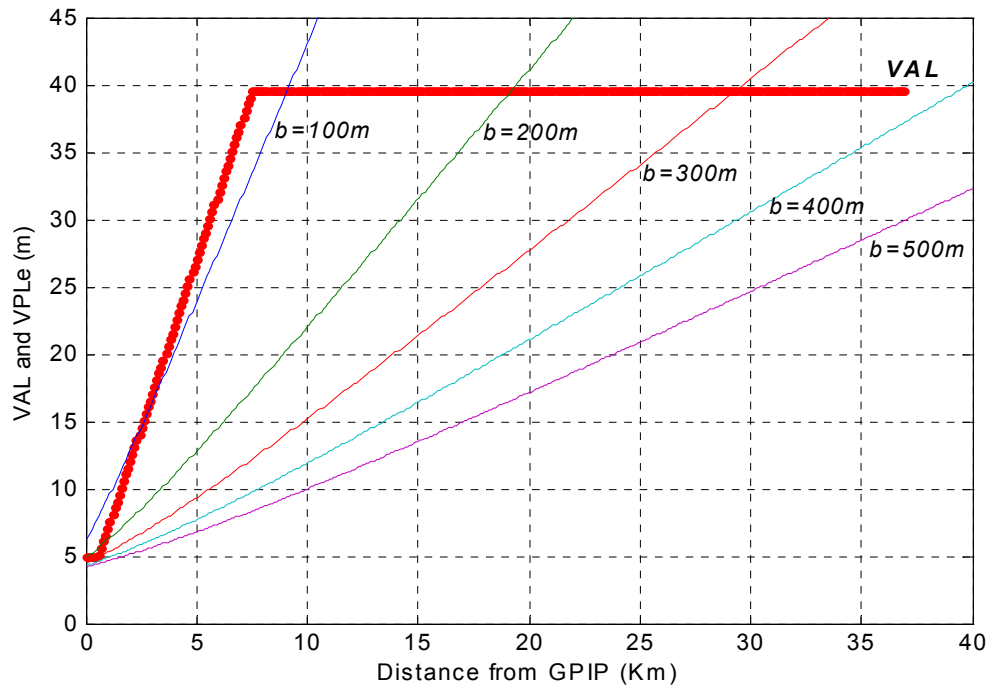


Figure 2.10 VPL_e Results for $x_0 = 1km$

A number of observations regarding the results are listed here:

- The required baseline length is highly dependent on the need to protect the entire 20nmi (about 37km) coverage volume. The “flat” region of VAL beyond 7.5 km is particularly constraining.
- In any case, the baseline length need not exceed 400 m. This requirement can probably be achieved on every airport property.
- There are two basic ways to reduce baseline length requirement: (1) Reduce the protected coverage volume. (2) Reduce the carrier-phase measurement error (σ_ϕ).

Taking a deeper look into the sensitivity of VPL_e to the parameters in equation (2-24), we see that near the origin of these graphs:

$$VPL_e |_{x_{a/c}=0} = VAL_{DH} \times K_2 \text{ (the intersection at the y axis when } x_{a/c} = 0 \text{)}$$

From the definition of $K_2 (= K_{mde} / K_{ff_md})$, the prior probability variation can change the value of y axis intersection. However, the coefficient K_2 is a weak function of the probability requirement P_{mde} and P_{ff_md} , there is little flexibility in performance in the “near-field” (i.e., near $x_{a/c} = 0$). The slope of each curve at $x_{a/c} = 0$ is:

$$\left. \frac{dVPL_e}{dx_{a/c}} \right|_{x_{a/c}=0} = K_1 \left(\frac{VAL_{DH}}{b} \right) \left(\frac{\sigma_{\Delta\phi}}{\sigma_{\Delta\rho}} \right) \quad (2-25)$$

From the definition of $K_1 (= K_{ffde} / K_{ff_md})$, we know that like K_2 , K_1 is also a weak function of the probability requirements. Therefore, if the probability requirements are released, the slope of each curve will not change significantly. The last two terms in Equation (2-25) are the inverse of baseline length and the noise ratio. They have equivalent influence power on the slope of each curve. This means if noise ratio between two signals can be reduced by a certain factor, it is equal to an increase in baseline length by the same factor.

CHAPTER III

DUAL FREQUENCY MONITOR ARCHITECTURE

The greatest disadvantage in the use of carrier phase measurements is that the integer ambiguity must be resolved correctly in order to get absolute range measurements. There are a number of different algorithms available for this purpose. We choose a geometry-free widelane method, because it is an approach that does not implicitly assume that the broadcast ephemeris is correct.

3.1 Widelane Observable Using Dual Frequency

Fundamental to the widelane method are the properties that the carrier cycle ambiguity is an integer and that the difference between carrier and code measurements provides a direct (but noisy) observation of the cycle ambiguity. If the code measurement error can be reduced to $\frac{1}{2}$ cycles of carrier phase or less, we can obtain the integer solution directly by rounding. Unfortunately the L1 and L2 carriers have very short wavelengths, so that reducing the noise floor of code measurements to $\frac{1}{2}$ cycles of these carriers is not possible. Clearly the problem would be made easier if the carrier wavelength were larger. The way to achieve this goal is to use the L1 and L2 carriers to construct a widelane band signal, L_w , with a longer wavelength. Using Equation (2-3), we define single difference carrier-phase measurements for two satellites (i and j):

$$\lambda_1 \Delta \phi_{ab}^i = \Delta R_{ab}^i + c \cdot (\delta t_b - \delta t_a) + \lambda_1 \Delta N_{ab}^i + \Delta v_\phi$$

$$\lambda_1 \Delta \phi_{ab}^j = \Delta R_{ab}^j + c \cdot (\delta t_b - \delta t_a) + \lambda_1 \Delta N_{ab}^j + \Delta v_\phi$$

A double difference equation can be obtain from subtracting the above two equations from each other:

$$\Delta^2 \phi_{ab}^{ij} = \frac{1}{\lambda_1} \Delta^2 R_{ab}^{ij} + \Delta^2 N_{ab}^{ij} + \frac{1}{\lambda_1} \Delta^2 v_{\phi} \quad (3-1)$$

In this section, the superscripts i, j and the subscripts a, b will be dropped to simplify notation. However, another subscript, 1 or 2 , is added to indicate carrier frequency L1 and L2 respectively.

Rewriting double difference carrier phase measurements taken in L1 and L2 bands:

$$\phi_1 = \frac{1}{\lambda_1} R + N_1 + \frac{1}{\lambda_1} \tilde{v}_{\phi_1} \quad (3-2)$$

$$\phi_2 = \frac{1}{\lambda_2} R + N_2 + \frac{1}{\lambda_2} \tilde{v}_{\phi_2} \quad (3-3)$$

where $\sigma(\tilde{v}_{\phi_2}) \approx \sigma(\tilde{v}_{\phi_1}) = 2\sigma(v_{\phi})$.

The widelane signal is constructed by subtracting Equation (3-3) from (3-2):

$$\begin{aligned} \phi_w &= \phi_1 - \phi_2 \\ &= R \left(\frac{1}{\lambda_1} - \frac{1}{\lambda_2} \right) + N_{12} + \tilde{v}_{\phi_{12}} \\ &= R \frac{1}{\lambda_w} + N_w + \frac{1}{\lambda_w} v_{\phi_w} \end{aligned} \quad (3-4)$$

where $\sigma(v_{\phi_w}) = 2\sqrt{2}\sigma(v_{\phi})$.

So the wavelength of widelane signal is:

$$\lambda_w = \frac{1}{1/\lambda_1 - 1/\lambda_2} = \frac{1}{f_1/c - f_2/c} = \frac{c}{f_1 - f_2} = 86.2 \text{ cm}$$

Note that the λ_w is about 4 times longer than L1 or L2 carrier wave lengths. We also can see its noise level is about 3 times higher than that of the raw L1 or L2 carriers.

3.2 Estimation of Carrier Cycle Ambiguities

One can process code measurements in the same manner, the double difference of L1 code measurements is:

$$\rho = R + \tilde{v}_\rho, \quad \sigma(\tilde{v}_\rho) = 2\sigma(v_\rho) \quad (3-5)$$

Recall that the L2 code is not available for civil use; fortunately, it is not needed for our purposes. We combine code measurements, in Equation (3-5), and widelane measurements, in Equation (3-4), to estimate integer N_w :

$$\left. \begin{array}{l} \lambda_w \phi_w = R + \lambda_w N_w + v_{\phi_w} \\ \rho = R + \tilde{v}_\rho \end{array} \right\} \Rightarrow \hat{N}_w = \phi_w - \frac{\rho}{\lambda_w} \quad (3-6)$$

The error on the widelane integer estimate has variance:

$$\sigma^2(\hat{N}_w) = \sigma^2(\tilde{v}_{\rho\phi_w}) = \frac{1}{\lambda_w^2} (\sigma^2(\tilde{v}_\rho) + \sigma^2(v_{\phi_w})) = \frac{1}{\lambda_w^2} (4\sigma^2(v_\rho) + 8\sigma^2(v_\phi))$$

Assuming for the moment that we obtain the correct integer via $N_w = \text{round}(\hat{N}_w)$,

we can then estimate N_l ($\Delta^2 N_{ab}^{ij}$ for L1) by solving the equations below:

$$\left\{ \begin{array}{l} N_1 - N_2 = N_w \\ N_1 - \frac{\lambda_2}{\lambda_1} N_2 = \phi_1 - \frac{\lambda_2}{\lambda_1} \phi_2 + \tilde{v}_{\phi_{12}} \end{array} \right. \Rightarrow \hat{N}_1 = \left(\frac{\lambda_2}{\lambda_1} - 1 \right)^{-1} \left[\frac{\lambda_2}{\lambda_1} N_w - \left(\phi_1 - \frac{\lambda_2}{\lambda_1} \phi_2 \right) \right] \quad (3-7)$$

where $\sigma(\tilde{v}_{\phi_{12}}) = \frac{1}{\lambda_1} (4\sigma^2(v_{\phi_1}) + 4(\frac{\lambda_2}{\lambda_1})^2 \sigma^2(v_{\phi_2}))^{\frac{1}{2}} = \frac{\sqrt{10.59}}{\lambda_1} \sigma(v_\phi)$,

and $\sigma(\hat{N}_1) = \left(\frac{\lambda_2}{\lambda_1} - 1 \right)^{-1} \frac{\sqrt{10.59}}{\lambda_1} \sigma(v_\phi) \approx \frac{11.5}{\lambda_1} \sigma(v_\phi)$

Now, with the process by which \hat{N}_w and \hat{N}_1 are defined in hand, we turn attention to determining the probabilities that \hat{N}_w and \hat{N}_1 are correct (that is, equal to N_w and N_1 , respectively). More practically, one may ask how many independent measurements need to be averaged in order to ensure that \hat{N}_w and \hat{N}_1 are correct, subject to specific probability requirements for incorrect solution.

Basically, the performance of estimation of \hat{N}_w relies on the noise floor of $\sigma(\tilde{v}_{\rho\phi w})$. If $\sigma(\tilde{v}_{\rho\phi w})$ can be reduced, one can expect a higher probability that $\hat{N}_w = N_w$. In this regard, the average of a sequence of \hat{N}_w s (obtained using independent measurements) can be taken over a finite time period to reduce $\sigma^2(\hat{N}_w)$ to meet a given probability requirement. The averaging time required to obtain the correct integer is an index of estimation performance. The standard deviation of averaged \hat{N}_w is:

$$\sigma_{w/ave} = \frac{\sigma(\hat{N}_w)}{\sqrt{n_w}}$$

where n_w is the total number of independent \hat{N}_w estimates during the averaging time.

Assume now a minimum probability requirement $P(R_{N_w})$ for the correct resolution of N_w . Given $\sigma_{w/ave}$, the equation below must be satisfied in order to get an acceptable integer solution:

$$P(|\tilde{v}_{N_w/ave}| < \frac{1}{2} \text{cycle}) > P(R_{N_w})$$

or equivalently:

$$K_w \times \sigma_{w/ave} \leq \frac{1}{2} \text{cycle} \quad (3-8)$$

where K_w is a multiplier corresponding to the probability $P(R_{N_w})$ assuming a standard normal distribution.

The same procedure is applicable to N_1 with a probability requirement $P(R_{N_1})$ - or equivalently, probability multiplier K_l and $\sigma_{1/ave}$ (the standard deviation of the \hat{N}_1 average):

$$P(|\tilde{\nu}_{N_1/ave}| < \frac{1}{2} cycle) > P(R_{N_1})$$

$$K_1 \times \sigma_{1/ave} \leq \frac{1}{2} cycle \quad (3-9)$$

$$\sigma_{1/ave} = \frac{\sigma(\hat{N}_1)}{\sqrt{n_1}} \quad (3-10)$$

where n_1 is the total number of independent \hat{N}_1 estimates obtained during the average time.

In order to proceed, the probability requirements for correct integer resolution \hat{N}_w and \hat{N}_1 have to be defined. These requirements can be derived from the specifications of Category III LAAS.

Probability Requirement Allocation for Cycle Resolution. Before describing how to allocate probability requirements for cycle resolution, it is first necessary to understand in more detail how the system will monitor satellite ephemeris errors. Returning to the double difference carrier phase measurement, Equation (3-1), in the L1 band, we have:

$$\Delta^2 \phi_{ab}^{ij} = \frac{1}{\lambda} \Delta^2 R_{ab}^{ij} + \Delta^2 N_{ab}^{ij} + \Delta^2 v_{\phi}$$

where $\Delta^2 R_{ab}^{ij} = \Delta R_{ab}^i - \Delta R_{ab}^j = (e_a^i)^T x_b - (e_a^j)^T x_b = [(e_a^i)^T - (e_a^j)^T] x_b$

Consider first the case where no ephemeris error exists and $\Delta^2 N_{ab}^{ij}$ has been correctly resolved using the technique described above; the residual of the double difference is:

$$\Delta^2 \phi_{ab}^{ij} - \frac{1}{\lambda} [(e_a^i)^T - (e_a^j)^T] x_b - \Delta^2 N_{ab}^{ij} = \Delta^2 v_\phi \quad (3-11)$$

This double difference residual, $\Delta^2 v_\phi$, is the combination of the residual errors primarily due to multipath and receiver noise.

Assume now that there exists a large ephemeris error on satellite j . In this case, the residual is:

$$\Delta^2 \phi_{ab}^{ij} - \frac{1}{\lambda} [(e_a^i)^T - (e_a^j)^T] x_b - \Delta^2 N_{ab}^{ij} = (\delta e_a^j)^T x_b + \Delta^2 v_\phi$$

where $e_a^j(\text{broadcast}) = e_a^j(\text{true}) + \delta e_a^j$

Here the magnitude of the residual ($|(\delta e_a^j)^T x_b + \Delta^2 v_\phi|$) will be larger than the nominal value ($|\Delta^2 v_\phi|$) without ephemeris error. Therefore, a threshold can be set on the residual as a checking standard for ephemeris error. When the residual value is bigger than the threshold, the system will trigger an alarm to warn the users to exclude the dangerous satellite. There exists three possible situations that can trigger an alarm:

1. Ephemeris error exists (correct alarm).
2. Large signal noise occurs (FA = false alarm).
3. Wrong integer estimation (FA).

Ideally, we want to set a threshold that is high enough to minimize false alarms, but also low enough to provide acceptable ephemeris error detection performance. The probability of false alarm can be broken down as follows:

$$\begin{aligned}
& P(\text{FA due to ephemeris monitor}) \\
&= P(\text{FA} \mid \text{wrong integer}) \cdot P(\text{wrong integer}) \\
&+ P(\text{FA} \mid \text{right integer}) \cdot P(\text{right integer})
\end{aligned}$$

Since it is desired that the $P(\text{wrong integer})$ be small, one may conservatively use $P(\text{right integer}) \approx 1$. In addition, $P(\text{FA} \mid \text{wrong integer}) \approx 1$ because with a wrong integer, the residual would exceed the threshold almost instantly. Under these assumptions, the above equation can be simplified as:

$$P(\text{FA due to ephemeris monitor}) = P(\text{wrong integer}) + P(\text{FA} \mid \text{right integer})$$

As explained in Chapter II, there are four fundamental parameters which provide the basis for allocation of specific requirements. They are *accuracy*, *integrity*, *availability* and *continuity*. For our immediate purpose, only availability and continuity are relevant. A rising satellite will be declared *unavailable* for use by the LAAS reference station if the residual test fails immediately following cycle resolution. There are two situations in which this can occur (which were already described above):

1. The integer solutions are wrong. The probability of this situation is noted as $P(\text{wrong integer})$.
2. The integers are correct, but signal noise causes the residual to exceed the threshold. The probability of this situation is noted as $P(\text{FA} \mid \text{right integer})$.

For Cat. III LAAS, it is desired that [MASPS98]:

$$P(\text{unavailable}) = P(\text{wrong integer}) + P(\text{FA} \mid \text{right integer}) \leq 10^{-4}$$

However, the residual test is executed throughout a satellite pass (after initial approval of the satellite), so that $P(\text{FA} \mid \text{right integer})$ is also constrained by continuity requirements. This is true because once a satellite was declared as available by the system, a

subsequent false alarm will terminate usage of the satellite. Therefore, the probability of false alarm given the right integer must be consistent with the continuity requirement for Cat. III LAAS (approximately 1×10^{-7}):

$$P(\text{FA} \mid \text{right integer}) \leq 10^{-7} \text{ to ensure continuity.}$$

while $P(\text{wrong integer}) \leq 10^{-4}$ to ensure availability (since $P(\text{FA} \mid \text{right integer}) \ll 10^{-4}$).

The fault detection threshold T_s is set using the continuity requirement as follows:

$$T_s = K_{ffde} \sigma(\Delta^2 v_\phi) = K_{ffde} 2\sigma(v_\phi) \quad (3-12)$$

where K_{ffde} shown in Equation (2-17) is chosen such that:

$$P(|\Delta^2 v_\phi| > K_{ffde} \sigma(\Delta^2 v_\phi)) < 10^{-7} \Rightarrow K_{ffde} = 5.33 \quad (3-13)$$

The threshold is then:

$$T_s = 5.33 \times 2\sigma(v_\phi) = 10.66\sigma(v_\phi) \quad (3-14)$$

The probability of incorrect integer resolution can be divided into two parts:

$$P(\text{wrong integer}) = P(\hat{N}_w \text{ wrong}) + P(\hat{N}_1 \text{ wrong} \mid \hat{N}_w \text{ right}) \cdot P(\hat{N}_w \text{ right})$$

Again, one can conservatively assume $P(\hat{N}_w \text{ right}) \approx 1$, so that:

$$P(\text{wrong integer}) = P(\hat{N}_w \text{ wrong}) + P(\hat{N}_1 \text{ wrong} \mid \hat{N}_w \text{ right})$$

It is now convenient to define a leverage variable a and allocate $P(\text{wrong integer})$ as follows:

$$P(\hat{N}_w \text{ wrong}) = a \cdot 10^{-4}$$

$$P(\hat{N}_1 \text{ wrong} \mid \hat{N}_w \text{ right}) = (1-a) \cdot 10^{-4}$$

where $0 < a < 1$. Therefore, a defines the actual probability allocation. In turn, for a given probability allocation, one can define the maximum acceptable standard deviations

of pseudorange and carrier phase measurements consistent with operationally acceptable initialization (averaging) times.

3.3 Range Measurement Error Requirements

Because the value of leverage variable a defines actual probability allocation between \hat{N}_w and \hat{N}_1 , the probability multipliers K_w and K_1 may be expressed directly as functions of a . Figure 4.1 shows the values of K_w and K_1 for values of a between 0.01 to 0.99.

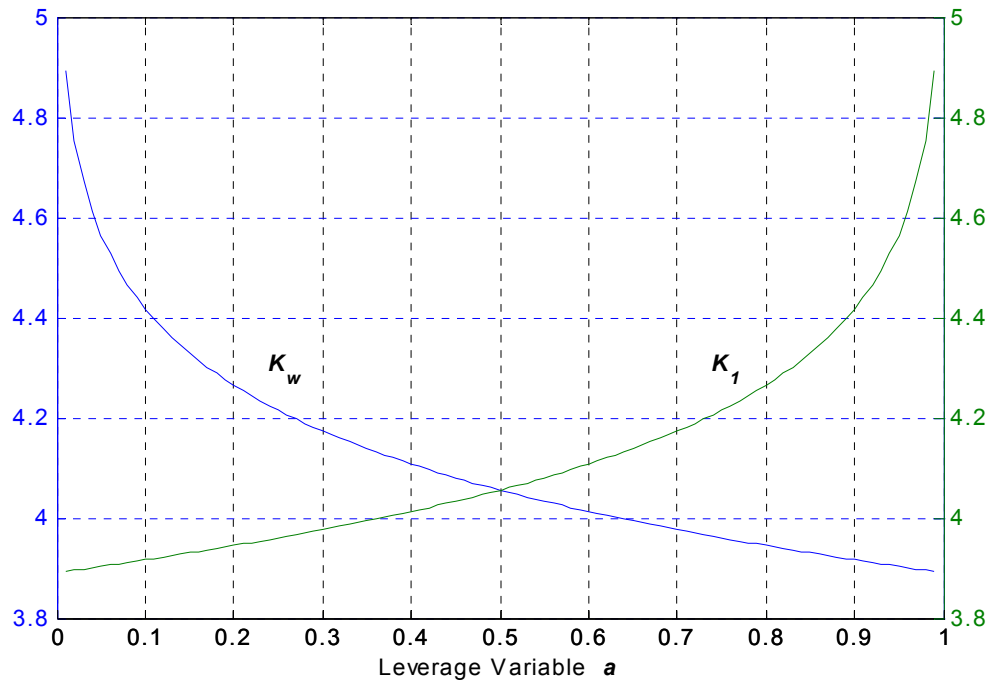


Figure 3.1 Probability Multipliers Variations

The number of independent measurement samples (initial time interval) required to estimate N_w and N_1 with the demanded probabilities of success can now be defined using the results of section 3.2. For the widelane integer, we have:

$$\begin{aligned}
K_w \times \sigma_{w/ave} &\leq \frac{1}{2} \text{cycles} \Rightarrow K_w \times \frac{[4\sigma^2(v_\rho) + 8\sigma^2(v_\phi)]^{\frac{1}{2}}}{\lambda_w \sqrt{n_w}} \leq 0.5 \\
\Rightarrow \sqrt{n_w} &\geq \frac{2K_w}{\lambda_w} \times (4\sigma^2(v_\rho) + 8\sigma^2(v_\phi))^{\frac{1}{2}} \\
\Rightarrow n_w &\geq \frac{16K_w^2}{\lambda_w^2} \times (\sigma^2(v_\rho) + 2\sigma^2(v_\phi)) \tag{3-15}
\end{aligned}$$

Likewise for the L1 integer:

$$\begin{aligned}
K_1 \times \sigma_{1/ave} &\leq \frac{1}{2} \text{cycles} \Rightarrow K_1 \times \frac{11.5\sigma(v_\phi)}{\lambda_1 \sqrt{n_1}} \leq 0.5 \\
\Rightarrow \sqrt{n_1} &\geq \frac{2K_1}{\lambda_1} \times 11.5\sigma(v_\phi) \\
\Rightarrow n_1 &\geq \frac{529K_1^2}{\lambda_1^2} \times \sigma^2(v_\phi) \tag{3-16}
\end{aligned}$$

The minimum time intervals (number of independent samples) n_w and n_1 both are functions of the probability multipliers and range measurement nominal standard deviations. The two probability multipliers may be eliminated in favor of the single leverage variable a .

First, we choose a set of fixed nominal values for the standard deviations to see the influence of the leverage variable a on n_w and n_1 : $\sigma(v_\rho) = 60$ cm and $\sigma(v_\phi) = 1$ cm. The results, shown in Figure 3.2, clearly show that n_w dominates the total initialization time. Therefore, the leverage variable $a = 0.99$ is chosen to minimize n_w .

With a selected, n_w and n_1 are functions of the standard deviations of the range measurements only. Figure 3.3 shows the needed waiting time (number of independent samples) for given standard deviation values of $\sigma(v_\phi)$ and $\sigma(v_{\rho\phi})$, where $\sigma(v_{\rho\phi}) = [\sigma^2(v_\rho) + 2\sigma^2(v_\phi)]^{1/2}$. In this figure, the x axis is a scale factor on the nominal

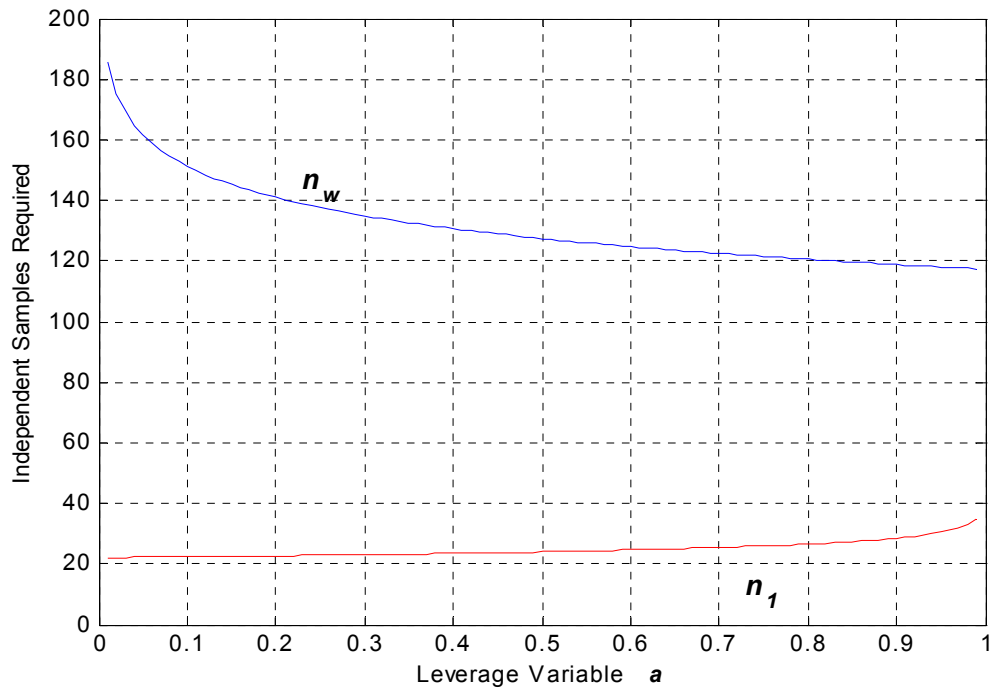


Figure 3.2 Initialize Waiting Time Intervals

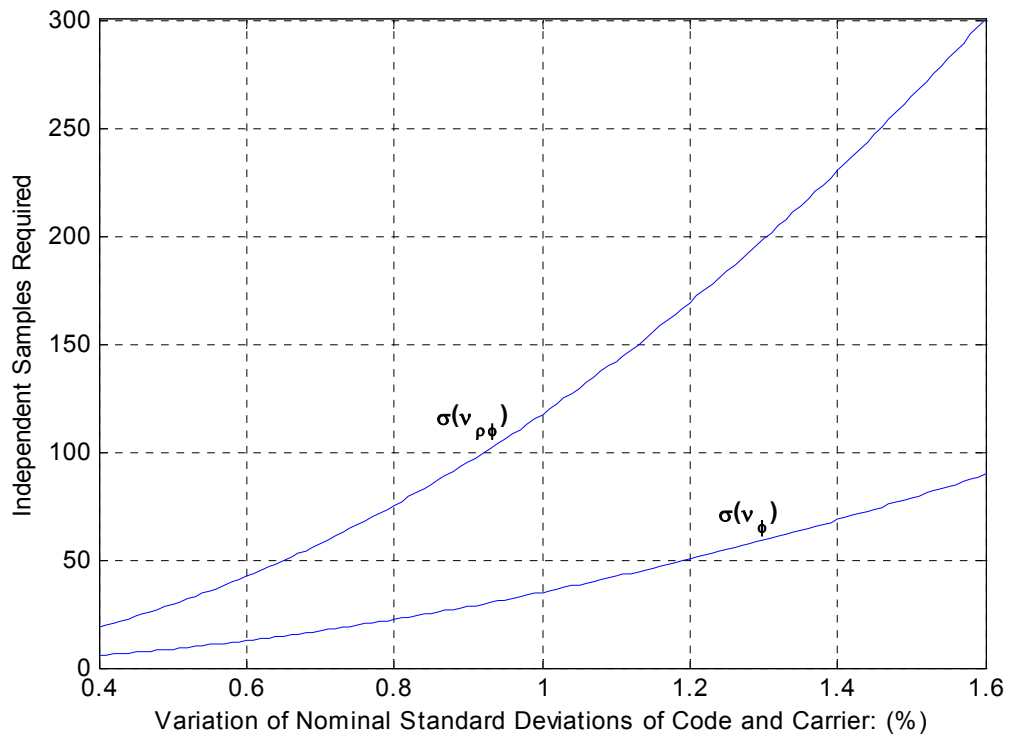


Figure 3.3 Relations between STD of Measurements and Number of Samples

standard deviations assumed in Figure 3.2 ($\sigma(v_{\rho\phi}) \approx \sigma(v_{\rho}) = 60$ cm and $\sigma(v_{\phi}) = 1$ cm).

Since the number of independent measurements to estimate N_w will be larger than the number of samples to estimate N_1 , only the N_w averaging time need to be considered further. Once N_w is determined, an ample number of measurements to estimate N_1 is also available. So integer N_1 can be resolved instantly.

The actual initialization time for a rising satellite is equal to number of independent measurements multiplied by the uncorrelated sampling interval. Both the code measurement noise and correlation time are satellite, environment and receiver dependent. In some cases, the actual initialization time required for rising satellites may differ from one another. Initialization time, code measurement standard deviations and uncorrelated sampling intervals are related as shown in Figure 4.4.

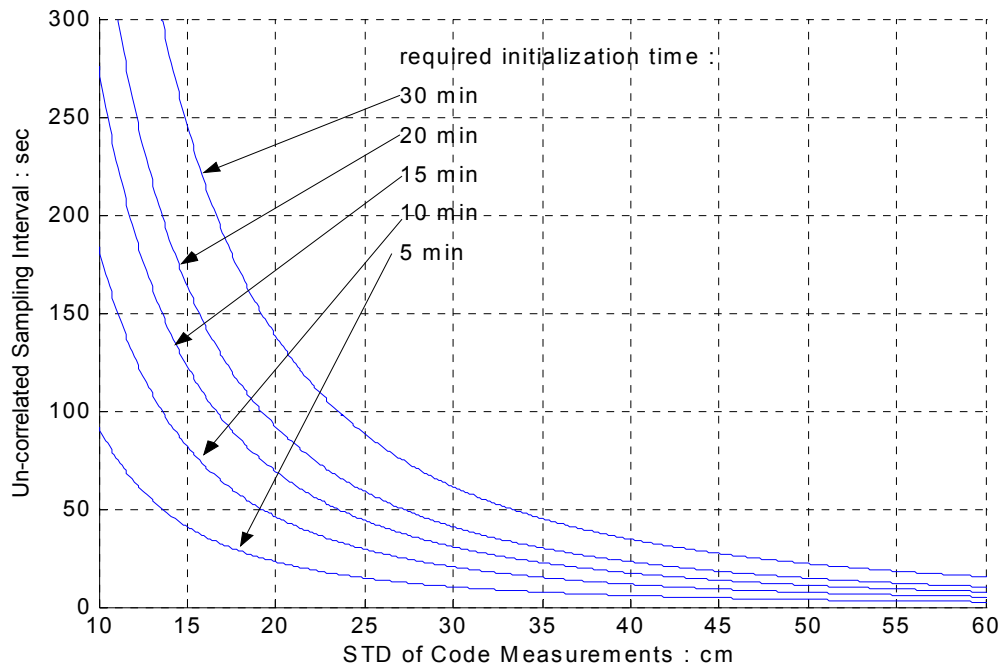


Figure 3.4 Relations between STD of Code measurements and Un-correlated Sampling Interval for Different Initialization Time.

In order to meet a short initialization time requirement (five minutes or less), the required standard deviation of the code measurements is lower than what can be obtained by using a normal GPS antenna. However, the performance of the Multipath Limiting Antenna (MLA) developed for LAAS Ground Facility (LGF) is sufficient in this regard [Warb99].

3.4 Preliminary Experiment and Results

To validate the ability to detect orbit ephemeris error based on this architecture and algorithm, L1 and L2 carrier-phase measurements and L1 code measurements were collected from two receivers on 3/19/2001. The receivers used were both NovAtel Millennium GPSCcard with ProPack II interface connected to L1/L2 GPS Choke Ring Antennas (Model 503). The antennas were located on the rooftop of the Engineering 1 Building at IIT, and were separated by a baseline of approximately 26 m.

The relative position of two antennas is shown in Figure 3.5. The antenna at the west side was chosen as the master antenna, so that baseline vector x_b was defined as a vector from west side antenna to east side antenna. Because the antennas are not MLA type, the error level of code measurements was not small enough to actually simulate a truly practical implementation of the algorithm, in the sense that the initialization times were long. The simulation data were processed in two stages. First, cycle ambiguity N_w was resolved by averaging 120 independent samples. Subsequently, N_1 were resolved instantly. The sampling period was determined in advance by examining time correlation of measurement error to ensure independent samples. Based on a first order Gauss-Markov model [Gelb74] and collected code measurement error data, a relatively conservative 150 second independent sampling interval was chosen.

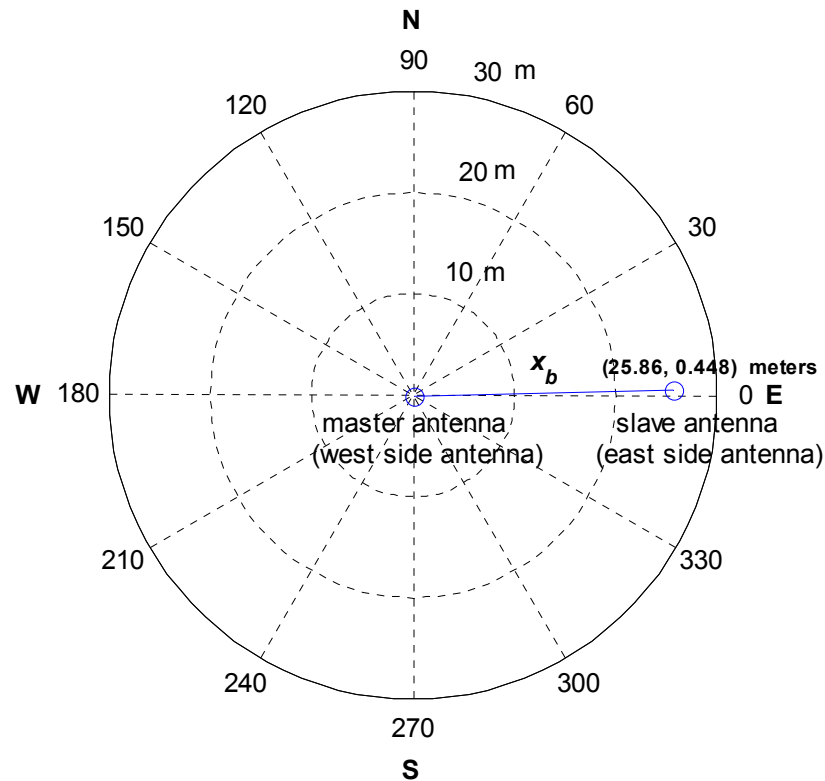


Figure 3.5 Relative Position of Two Antennas

For the second stage, the resolved cycle ambiguity N_1 was removed from the double difference of carrier-phase measurements to generate the residual for fault detection. An ephemeris error was later deliberately injected into the data.

Figure 3.6 shows the results without ephemeris error injection. The high noise magnitude during the periods at the beginning and end of the residual history correspond to low elevation angles for the satellite. This behavior is typical because the effect of multipath is more significant at low elevations. Therefore, the standard deviation of carrier measurement error is larger at low elevation angles. The variation of carrier error standard deviation versus elevation was quantified by Heo [Heo00]. Using Heo's results

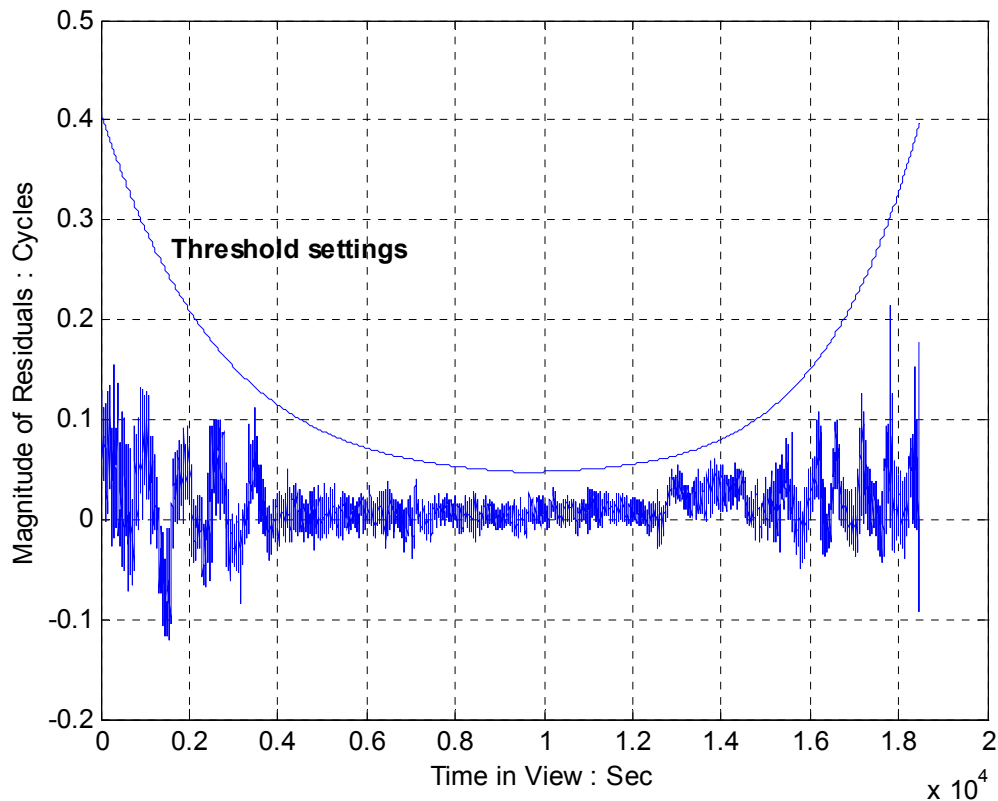


Figure 3.6 Residuals of Double Difference Carrier Phase Measurements

for standard deviation , together with Equation (3-11), gives the detection threshold curve shown in Figure 3.6. (the satellite pair used here is prn #17 and #26.)

Figure 3.7 shows the results with an ephemeris error injected 2 hours into the satellite pass. Here, the eccentricity was changed by adding 0.0003 to the original value. After error injection, the double difference carrier phase residual immediately exceeded the threshold setting, the ephemeris error was therefore detected. The injecting ephemeris error lasted two hours to simulate a real ephemeris update period. The actual satellite orbital position errors corresponding to this erroneous ephemeris are shown in Figure 3.8 (the time axes in Figure 3.7 and 3.8 are the same). Smaller orbit errors can

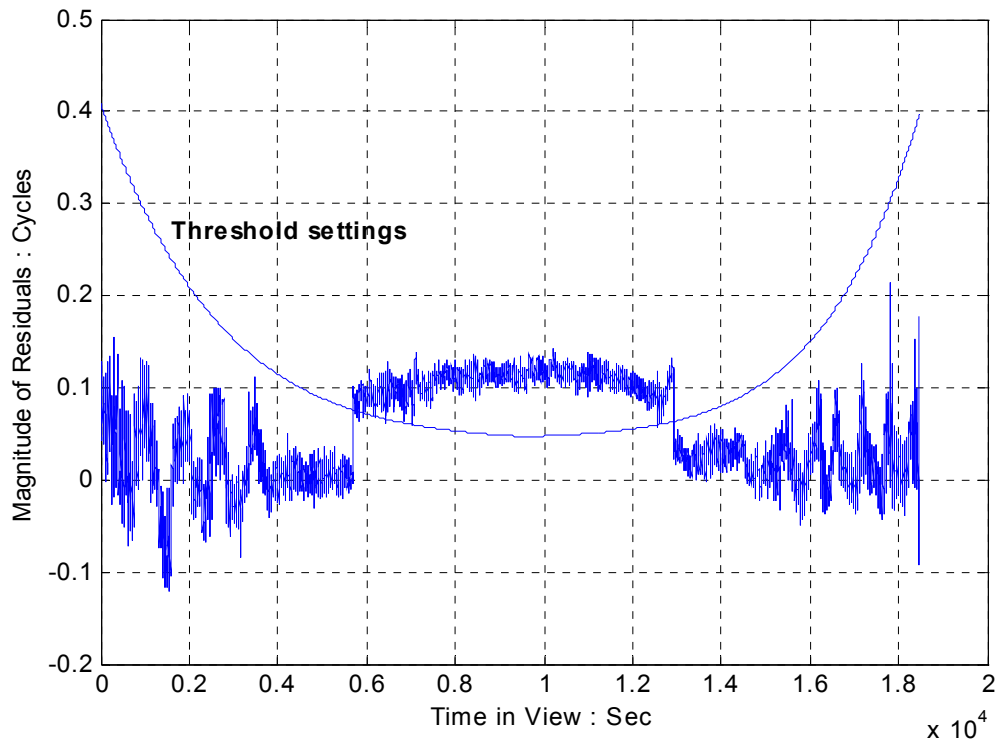


Figure 3.7 Carrier Residuals with Ephemeris Error Injection

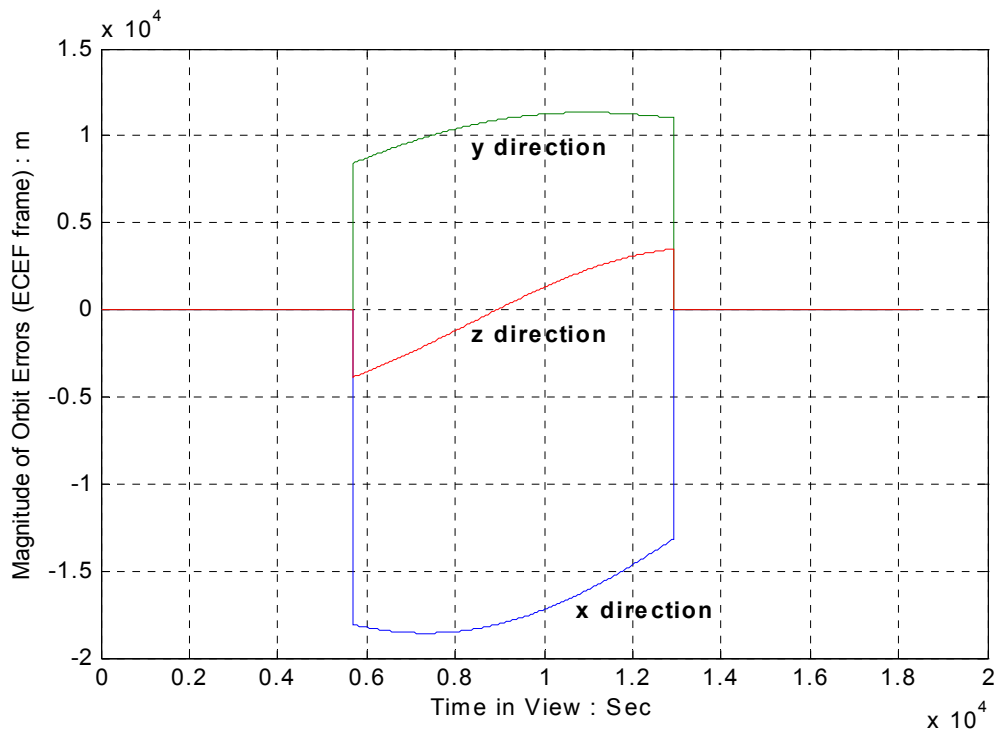


Figure 3.8 Orbital Position Errors due to Ephemeris Error

also be detected by this algorithm if a longer receiver antenna baseline is available. Recall that the algorithm performance versus baseline length was quantified in Section 2.3.

CHAPTER IV

SINGLE FREQUENCY APPROACHES TO EPHEMERIS MONITORING

The currently specified Category I LAAS Ground Facility (LGF) equipment only has ability to acquire and track the L1 band GPS signal. Therefore, the dual frequency monitor architecture proposed in previous chapter can not be implemented for Category III on the LGF without modification. For this reason, a number of different single frequency ephemeris monitoring algorithms have also been developed and evaluated with regard to their potential to meet the navigation requirements of Category III LAAS.

4.1 Pseudorange Differential Baseline Method

In Chapter II we derived the performance of an ephemeris integrity monitor which used carrier-phase measurements. In Chapter III we defined a dual-frequency approach to resolve carrier cycle ambiguities, so that the monitor performance could be realized. It may be noted that using pseudorange (code phase) measurements alone, cycle resolution is not required. And therefore, the second frequency is unnecessary.

In this context, we may ask whether the use of pseudorange measurements alone in the ephemeris monitor is more appropriate. The answer is no, because the pseudorange error is much larger in magnitude the carrier-phase error.

The performance of using pseudorange measurement can be easily quantified using equation (2-24) by changing the ratio $\sigma_{\Delta\phi} / \sigma_{\Delta\rho}$ to $\sigma_{\Delta\rho} / \sigma_{\Delta\rho} \equiv 1$. In this case, VPL_e bound can be defined as follows:

$$VPL_e \leq VAL_{DH} \left[K_1 \left(\frac{x_{a/c}}{b} \right) + K_2 \sqrt{\left(\frac{x_{a/c}}{b} \right)^2 + 1} \right] \quad (4-1)$$

Using the same parameter values as in Section 2.3, the VPL_e bound (4-1) was computed; the results are shown in Figure 4.1. Obviously, the performance is still not sufficient to cover the whole LAAS service volume even using a 7 km baseline length. Such a long baseline is not acceptable in any airport property.

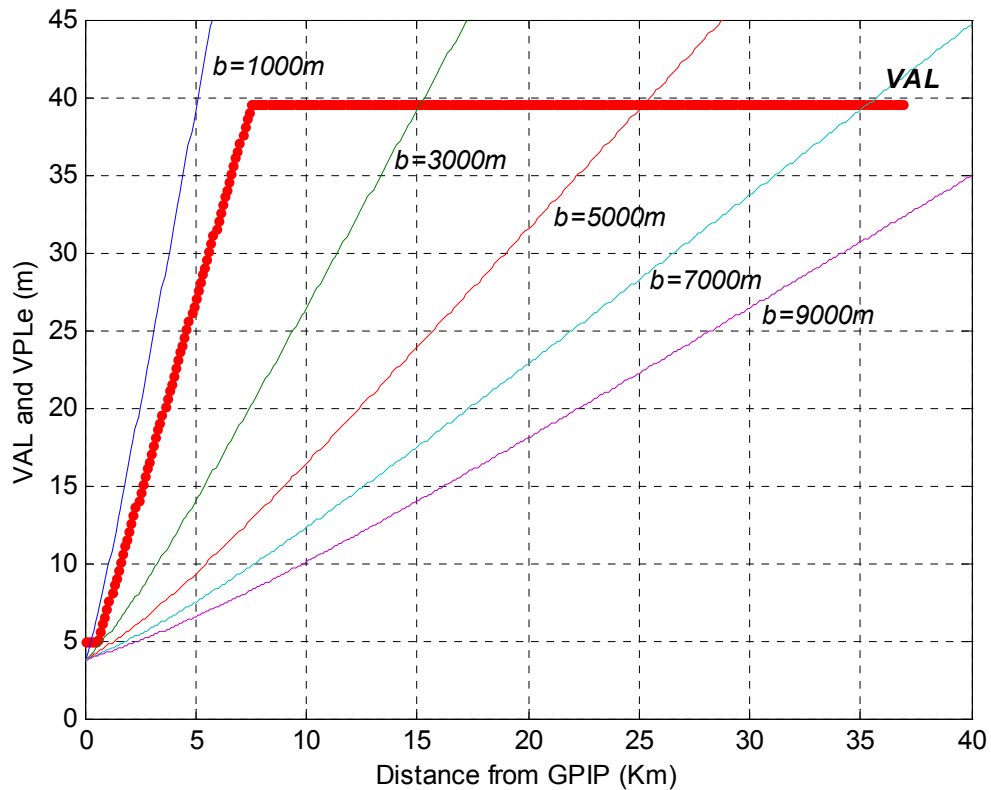


Figure 4.1 VPL_e Results for $x_0 = 0km$ Using Pseudorange Measurements

4.2 Time History Method by Using L1 Carrier Differential Baseline

Observing the relative time history of the carrier-phase residual can potentially alleviate the need for cycle resolution. Here, the basic idea is that an error in the orbit parameters will necessarily cause the carrier-phase residual to show a dynamic response

over time. Using equation (2-10), the normalized single differential ranging error at satellite rise time t_r is:

$$\frac{\delta\Delta\phi_{t_r}}{b} = F(t_r)^T \delta R_{t_r} \quad (4-2)$$

Where vector $F(t_r)$ is defined via projection along the direction of displacement of the baseline(b). Next, recall the observation Equation (3-1) for double difference carrier phase measurements:

$$\Delta^2\phi_{ab}^{ij} = \frac{1}{\lambda} \Delta^2 R_{ab}^{ij} + \Delta^2 N_{ab}^{ij} + \frac{1}{\lambda} \Delta^2 v_{\phi}$$

The superscripts i, j and the subscripts a, b are dropped to simplify notation, while the time epoch notation k is added as a subscript:

$$\Delta^2\phi_k = \frac{1}{\lambda_1} \Delta^2 R_k + \Delta^2 N + \frac{1}{\lambda_1} \Delta^2 v_{\phi k} \quad (4-3)$$

When an ephemeris error exists, the result of subtracting the $\Delta^2 R_k / \lambda_1$ term (computed using the erroneous broadcast ephemeris and known baseline) from double difference carrier-phase measurement is:

$$\begin{aligned} \Delta^2\phi_k - \frac{1}{\lambda_1} \Delta^2 R_k &= \frac{1}{\lambda_1} \delta e_k^T x_b + \Delta^2 N + \frac{1}{\lambda_1} \Delta^2 v_{\phi k} \\ &= \frac{1}{\lambda_1} \delta\Delta\phi_k + \Delta^2 N + \frac{1}{\lambda_1} \Delta^2 v_{\phi k} \end{aligned} \quad (4-4)$$

According the orbital mechanics, given some initial (small) deviation in satellite position and velocity (δR_0 and δV_0) from a circular orbit, future positions can be defined by the Euler-Hill transition matrix H_k [Bate71, Kaplan76]:

$$\delta R_k = H_k \begin{bmatrix} \delta R_0 \\ \delta V_0 \end{bmatrix} \equiv H_k \delta S_0 \quad (4-5)$$

To use the Euler-Hill transition matrix, δR_k , δR_0 , and δV_0 must be defined with respect to the reference orbit frame (radial, in-track, and cross-track directions).

We now define t as an arbitrary time corresponding to epoch index k and t_r as the satellite rise time. Equation (4-4) is then evaluated at both times to eliminate the cycle ambiguity and normalized with respect to the baseline length b . The difference of the two normalized double difference observables is called the normalized triple difference residual:

$$\begin{aligned} r^\phi(t) &= \frac{[\lambda_1 \Delta^2 \phi(t) - \Delta^2 R(t)] - [\lambda_1 \Delta^2 \phi(t_r) - \Delta^2 R(t_r)]}{b} \\ &= \frac{x_b^T [\delta e(t) - \delta e(t_r)] + \Delta^3 v_\phi}{b} \\ &= \frac{[\delta \Delta \phi(t) - \delta \Delta \phi(t_r)] + \Delta^3 v_\phi}{b} \end{aligned} \quad (4-5.1)$$

Substituting equation (4-2) into the result above and replacing orbit error δR_t by equation (4-5), the scalar function $s(t)$ is defined below to represent the relative time history of normalized triple differential carrier-phase residual due to ephemeris error above:

$$\begin{aligned} s(t) &\equiv \frac{\delta \Delta \phi(t) - \delta \Delta \phi(t_r)}{b} = \frac{x_b^T [\delta e(t) - \delta e(t_r)]}{b} \\ &= F(t)^T \delta R_t - F(t_r)^T \delta R_{t_r} \\ &= F(t)^T H(t-t_r) \delta S_{t_r} - F(t_r)^T \delta S_{t_r} \\ &= [F(t)^T H(t-t_r) - F(t_r)^T] \delta S_{t_r} \\ \Rightarrow s(t) &= c(t, t_r) \delta S_{t_r} \end{aligned} \quad (4-6)$$

where $c(t, t_r) = [F(t)^T H(t - t_r) - F(t_r)^T]$. Using Equation (4-2), we can also define the effective ranging error per unit baseline length (due to ephemeris error only) at time t :

$$r(t) = F(t)^T \delta R_t = F(t)^T H(t - t_r) \delta S_{t_r}$$

Define $d(t, t_r) \equiv F(t)^T H(t - t_r)$, so that:

$$r(t) = d(t, t_r) \delta S_{t_r} \quad (4-7)$$

If one can infer $r(t)$, the normalized ranging error across baseline b (which is not directly measurable because the cycle ambiguities are unknown), using $s(t)$ (which is measurable), then ephemeris error is indirectly observable. Since function $s(t)$ is just an offset version of function $r(t)$, by the magnitude of $r(t_r)$, these two functions have exactly the same shape except that they are separated by a fixed bias. This unknown fixed bias is associated with the unknown cycle ambiguities. If the ratio between $r(t_c)$ (normalized ranging error at current time t_c) and maximum value of $s(t)$ for $t < t_c$, is unity or smaller after a certain waiting time, the normalized ranging error will be bounded by $\|s(t)\|_\infty$ where t is smaller or equal to t_c . In this case the detection performance using $s(t)$, $t < t_c$, is equivalent to that obtained by using $r(t_c)$ when the cycle ambiguities are known.

The key to evaluate the time history method is to determine whether the ratio $|r/s|$ converges below one, and if so, how much time dose it take to do so. In this regard we seek the worst case ratio for a given satellite as follows:

$$\left| \frac{r}{s} \right|_{\text{worst}} \leq \sup_{t_f \geq t_c > t_r} \left\{ \sup_{\delta S_{t_r}} \left\{ \frac{|d(t_c, t_r) \delta S_{t_r}|}{\sup_{t_c > t > t_r} |c(t, t_r) \delta S_{t_r}|} \right\} \right\}$$

Where t_f is the final time of visibility.

Expressing $\sup_{t_c > t > t_f} |c(t, t_r) \delta S_{t_r}|$ using a matrix form $C = \begin{bmatrix} c(t_c, t_r) \\ c(t_{c-1}, t_r) \\ \vdots \\ c(t_{r+1}, t_r) \end{bmatrix}$, the ratio is:

$$\left| \frac{r}{s} \right|_{\text{worst}} \leq \sup_{t_c} \left\{ \sup_{\delta S_{t_r}} \left\{ \frac{|d(t_c, t_r) \delta S_{t_r}|}{\|C \delta S_{t_r}\|_{\infty}} \right\} \right\}$$

Given that C matrix has full column rank, we may write:

$$\begin{aligned} \left| \frac{r}{s} \right|_{\text{worst}} &\leq \sup_{t_c} \sup_{\delta S_{t_r}} \frac{\|d(C^T C)^{-1} C^T C \delta S_{t_r}\|_{\infty}}{\|C \delta S_{t_r}\|_{\infty}} \leq \sup_{t_c} \sup_{\delta S} \frac{\|d(C^T C)^{-1} C^T\|_1 \|C \delta S_{t_r}\|_{\infty}}{\|C \delta S_{t_r}\|_{\infty}} \\ &\Rightarrow \left| \frac{r}{s} \right|_{\text{worst}} < \sup_{t_c} \|d(C^T C)^{-1} C^T\|_1 \end{aligned}$$

Simulation results for a Chicago O'Hare airport LGF installation using the DO-229A GPS constellation is shown in Figure 4.2.

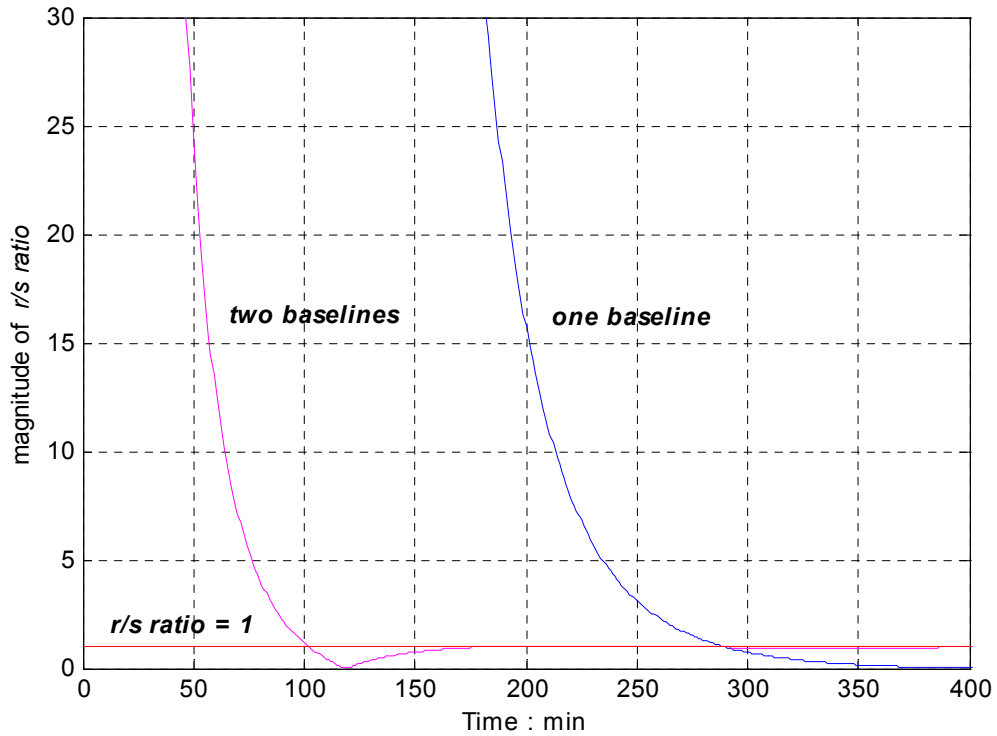


Figure 4.2 Worst Case r/s Ratio VS. Time

The ground configuration for this simulation consists of two perpendicular baselines with a receiver at each baseline end. One baseline is aligned toward east (the aircraft approach direction) and the other toward north. The simulation results show the r/s ratio does converge but the time needed is quite long. The convergence time will vary somewhat with the location of reference receivers on the earth and the particular satellite used. However, given that the simulation scenario is most likely not a worst case, it is evident that the use of the relative time history of the carrier residual is not an acceptable alternative for real-time use.

The results from the last two sections suggest that *real-time* detection of orbit errors will require resolution of cycle ambiguities. There are many approaches toward resolving the carrier cycle ambiguities, some of which exploit satellite geometry. As noted in the last chapter, these methods are undesirable because they implicitly rely on the validity of the broadcast ephemeris. The geometry-free widelane method defined in the previous chapter to resolve integer ambiguity is an appropriate solution to this problem. The cost of this technique, however, is that both L1 and L2 band carrier signals must be available to construct an artificial signal, called widelane band signal. It is an unfortunate fact, however, that as currently specified LAAS ground receivers have no capability to track L2 band signal. Therefore, the proposed ephemeris monitoring architecture defined in Chapters II and III is a candidate solution for future Category II/III implementation, but not a currently realizable implementation for LAAS system.

With a single frequency system, however, a more limited detection capability – effective against Type B ephemeris failures - is possible. We will discuss this in more detail in the following section.

4.3 Pseudorange Residual Method

In the first two sections of this chapter, alternative methods using single frequency measurements were explored with the goal of detecting orbit errors in real-time without the need for cycle ambiguity resolution. The results fell short of this goal. Here, we relax the problem to a certain extent and consider Type B (Class B) ephemeris failures only. In this case, “new ephemeris” minus “old ephemeris” test (an existing ephemeris monitoring method implemented in ground reference station for Category I LAAS) described in Chapter I is a sufficient solution provided that a valid old ephemeris is always available.

In this context, we need only consider validating an ephemeris following a scheduled satellite stationkeeping maneuver. Recall that unscheduled maneuvers are Type A failures which are excluded by hypothesis here. More further, because stationkeeping maneuvers are infrequent, it is not unreasonable to assume that a longer period of data collection (perhaps a day) will be acceptable to validate a post-maneuver ephemeris. In this regard we ask, given one day of measurement data, is it possible to observe orbit error in an effective way? The answer is yes. Because over a longer period, the dynamic response to the orbit error will be more clearly observable. We will first consider the use of pseudorange measurements only. In the next section, single frequency carrier-phase measurement will be added.

In a DGPS ground reference station, a pseudorange correction is formed for broadcast to users in the service volume. We refer to the correction here as “pseudorange residual”, because it contains all residual errors including ephemeris error:

$$r_k^p = e_k^T \delta R_k + v_k^p \quad (4-8)$$

where r_k^ρ is the pseudorange residual at time epoch k , $e_k^T \delta R_k$ is the orbit error (δR_k) in ranging component, v_k^ρ is the pseudorange measurement error. Note that no ground baseline is involved in the pseudorange residual defined by (4-8). As a result, the measurement error v_k^ρ will include the effects of satellite clock error, ionosphere error, troposphere error, as well as multipath and receiver noise (the last two are also experienced in the single difference case).

Using the Euler-Hill transition matrix [equation (4-5)], equations (4-8), the pseudorange residual is:

$$r_k^\rho = e_k^T H_k \delta S_0 + v_k^\rho = u_k \delta S_0 + v_k^\rho \quad (4-9)$$

where $u_k \equiv e_k^T H_k$.

Stacking the pseudorange residual for the entire day, one can obtain a least squares estimate of initial orbit error in terms of the pseudorange residual and unknown measurement error:

$$\begin{bmatrix} r_1^\rho \\ \vdots \\ r_n^\rho \end{bmatrix} = \begin{bmatrix} u_1 \\ \vdots \\ u_n \end{bmatrix} \delta S_0 + \begin{bmatrix} v_1^\rho \\ \vdots \\ v_n^\rho \end{bmatrix} \Rightarrow R_\rho = U \delta S_0 + v^\rho$$

$$\delta S_0 = (U^T U)^{-1} U^T R_\rho + (U^T U)^{-1} U^T v^\rho \quad (4-10)$$

The first term on the right hand side of Equation (4-10) represents an estimated value of δS_0 . The second term represents the estimate error due to measurement noise.

At the an arbitrary time epoch k the next day, the computed ranging error using the prior day's ephemeris for a landing aircraft at position $[x_1 \ x_2] b_{a/c}$ is using equation (2-10):

$$\delta \Delta \phi = b_{a/c}^T F_k H_k \delta S_0 = b_{a/c}^T A_k \delta S_0 \quad (4-11)$$

where x_1 and x_2 are column unit vectors defining the reference receiver baseline

direction; $b_{a/c}$ is the distance (column) vector whose elements are the displacements in each baseline unit vector directions x_1 and x_2 ; and $A_k \equiv F_k H_k$.

The significance of defining ranging error due to the prior day's ephemeris is that we want to use this ephemeris to validate the current day's ephemeris, but we need to first determine quantitatively how effective we should expect such a comparison to be. In this regard the variance of estimated ranging error is:

$$\begin{aligned}
& E\{b_{a/c}^T A_k (U^T U)^{-1} U^T v^\rho [b_{a/c}^T A_k (U^T U)^{-1} U^T v^\rho]^T\} \\
&= E[b_{a/c}^T A_k (U^T U)^{-1} U^T v^\rho v^{\rho T} U (U^T U)^{-1} A_k^T b_{a/c}] \\
&= b_{a/c}^T A_k (U^T U)^{-1} U^T E[v^\rho v^{\rho T}] U (U^T U)^{-1} A_k b_{a/c} \\
&= b_{a/c}^T A_k (U^T U)^{-1} U^T U (U^T U)^{-1} A_k^T b_{a/c} \sigma_{v^\rho}^2 \\
&= b_{a/c}^T A_k (U^T U)^{-1} A_k^T b_{a/c} \sigma_{v^\rho}^2 \leq \|A_k (U^T U)^{-1} A_k^T\|_2 \|b_{a/c}\|_2^2 \sigma_{v^\rho}^2
\end{aligned} \tag{4-12}$$

In the LAAS community, it is customary to define a “ P -value” to quantify the effectiveness of an orbit detection scheme:

$$P = \frac{MDE_i}{R_a^i} \tag{4-13}$$

where MDE_i is the minimum detectable orbital position error magnitude for satellite i , R_a^i is the range between receiver a and satellite i . The effective P -value associated with orbit error observability at time epoch k during initialization is:

$$P_{eff_k} = (K_{ffd_e} + K_{md_e}) \|A_k (U^T U)^{-1} A_k^T\|_2^{\frac{1}{2}} \sigma_{v^\rho} \tag{4-14}$$

Figure 4.3 shows simulation results for a Chicago O’Hare LGF installation. The different traces in the figure are associated with different satellite passes. In this simulation, the following data were used:

- $\sigma_{\nu\rho} = 10m$ (standard deviation of pseudorange measurement error – non differential).
- $(K_{ffde} + K_{md_e}) = 8.5$ (for Category I)
- DO-229A constellation, with a 5 deg elevation mask.

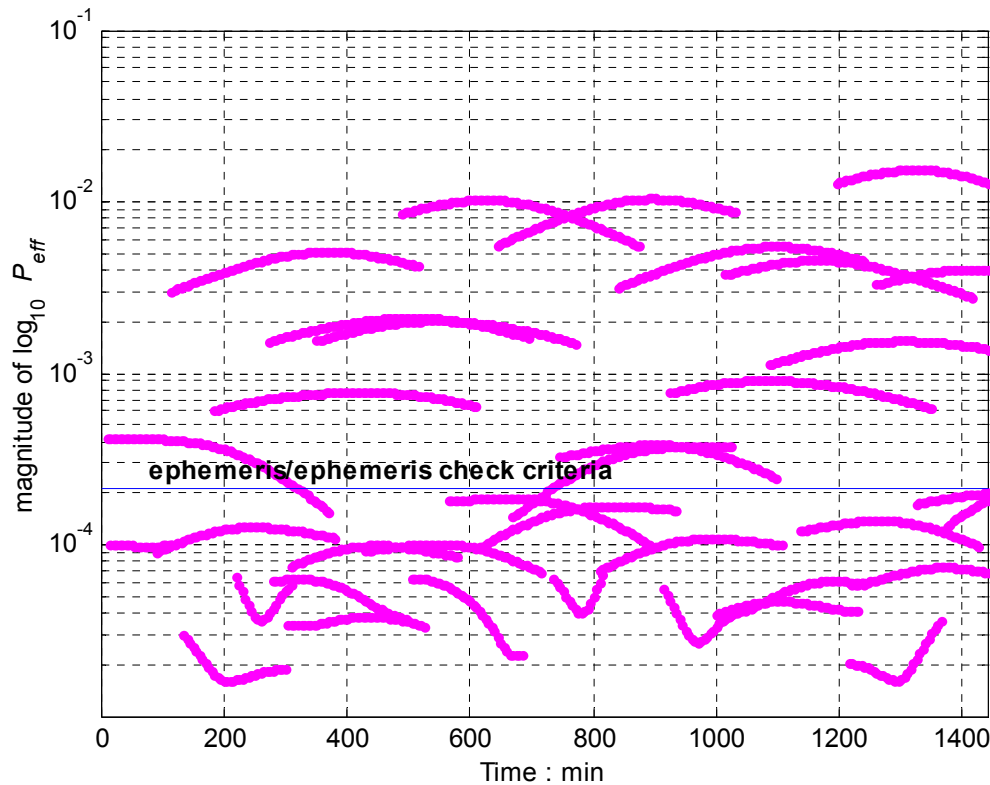


Figure 4.3 Simulation Results of P_{eff} Values by Pseudorange Measurements

For comparison, the expected performance of the ephemeris minus ephemeris test [PT1LAAS, ICD-200] is shown in the figure. At a minimum, we desire P_{eff} to be at (or below) this level for our ephemeris initialization process to be effective.

It is evident, however, that the results using pseudorange residual measurements alone are not always good enough to meet ephemeris/ephemeris check criteria. In this regard, we will now introduce carrier-phase measurements to estimate initial orbit error.

4.4 Carrier-phase Measurement Residual Method

We begin with the triple difference carrier-phase residual from Equation (4-5.1) without normalization:

$$r_k^\phi = bx_1^T [\delta e_k - \delta e_0] + \Delta^3 v_k^\phi \quad (4-15)$$

where we have replaced the time variable t with time epoch index k ; δe_k is the line-of-sight unit vector error at time epoch k ; x_1 is the unit baseline direction vector; b is the scalar baseline length; and $\Delta^3 v_k^\phi$ is the triple difference measurement error. Now we add another baseline, bx_2 , perpendicular to previous one with the same length b in order to detect all orbit error components lying on the plane perpendicular to line-of-sight vector, and normalize the residual with respect to baseline length b . The normalized carrier residual vector (2×1) can be expressed as:

$$\tilde{r}_k^\phi = \frac{r_k^\phi}{b} = \begin{bmatrix} x_1^T \\ x_2^T \end{bmatrix} [\delta e_k - \delta e_0] + \frac{\Delta^3 v_k^\phi}{b} = [F_k^T H_k - F_0^T H_0] \delta S_0 + \frac{\Delta^3 v_k^\phi}{b} = c_k \delta S_0 + \frac{\Delta^3 v_k^\phi}{b}$$

where c_k was defined in equation (4-6).

In the same manner as the pseudorange residual, it is possible to stack up this normalized carrier residual for one day to obtain the estimate of initial orbit error δS_0 :

$$\delta S_0 = (C^T C)^{-1} C^T R_\phi + (C^T C)^{-1} C^T \frac{\Delta^3 v^\phi}{b} \quad (4-16)$$

And the variance of the estimate ranging error due to carrier-phase measurement noise for a landing aircraft at the position $[x_1 \ x_2] b_{a/c}$ can be expressed:

$$\sigma_{r^\phi}^2 = b_{a/c}^T C_k (C^T C)^{-1} C_k^T b_{a/c} \frac{\Delta^3 \sigma_\phi^2}{b^2} \leq \|C_k (C^T C)^{-1} C_k^T\|_2^2 \|b_{a/c}\|_2^2 \frac{\Delta^2 \sigma_\phi^2}{b^2} \quad (4-17)$$

The effective p -value associated with this case is then:

$$P_{eff} = (K_{ffd_e} + K_{md_e}) \left\| C_k (C^T C)^{-1} C_k^T \right\|_2 \frac{2\sigma_\phi}{b} \quad (4-18)$$

Figure 4.4 shows the simulation results using the triple differential carrier-phase residuals for a Chicago O'Hare LGF installation. The assumptions are the same as those used to generate Figure 4.3 except the standard deviation of carrier-phase measurement error σ_ϕ is assumed to be 0.01 m, and an additional baseline length parameter is equal to 100 m.

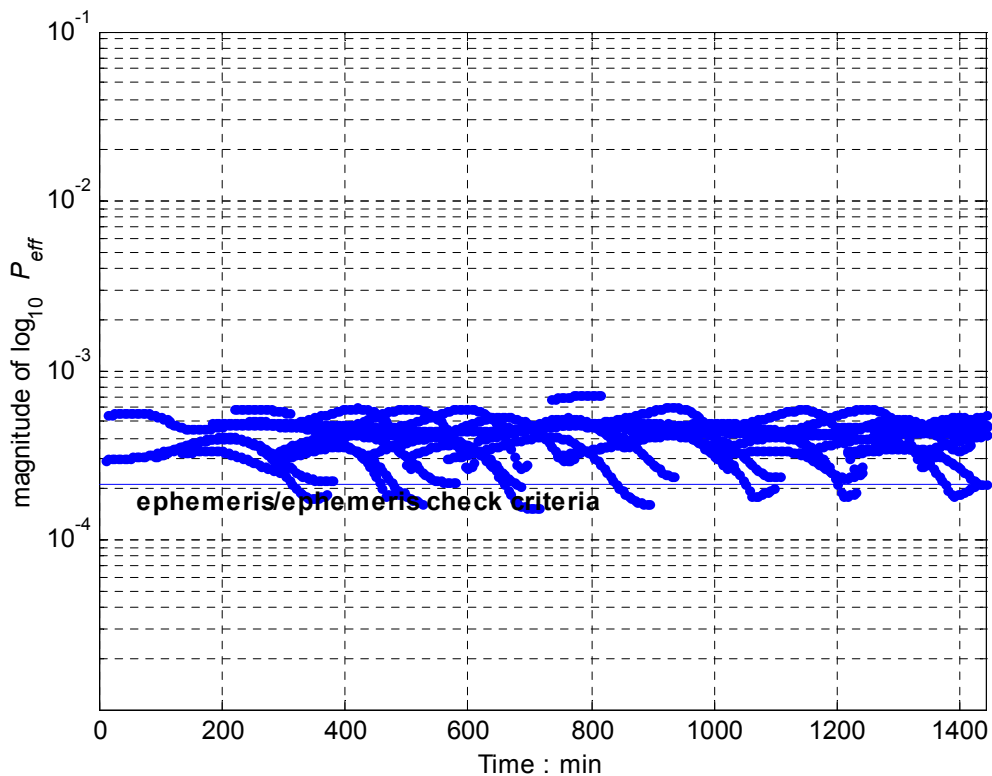


Figure 4.4 Simulation Results of P_{eff} Values by Carrier Measurements

The results in Figure 4.4 are still not quite good enough to meet the ephemeris/ephemeris check criteria. Further improvement is possible, however, by combining the pseudorange residual measurements with the carrier-phase residuals. Figure 4.5 shows that the results using both types of residuals is sufficient to meet the

ephemeris/ephemeris check criteria. The reason that the combination of the two residuals works better is that the combined residual stack effectively measures all components of orbit error. If either pseudorange residuals or carrier residuals are used alone, one or two components of orbit error may be only weakly observable. Since the combined residual performance is consistent with that of the ephemeris/ephemeris test, it is a viable solution to initialize the ephemeris/ephemeris test when there is no pre-approved valid ephemeris data exists.

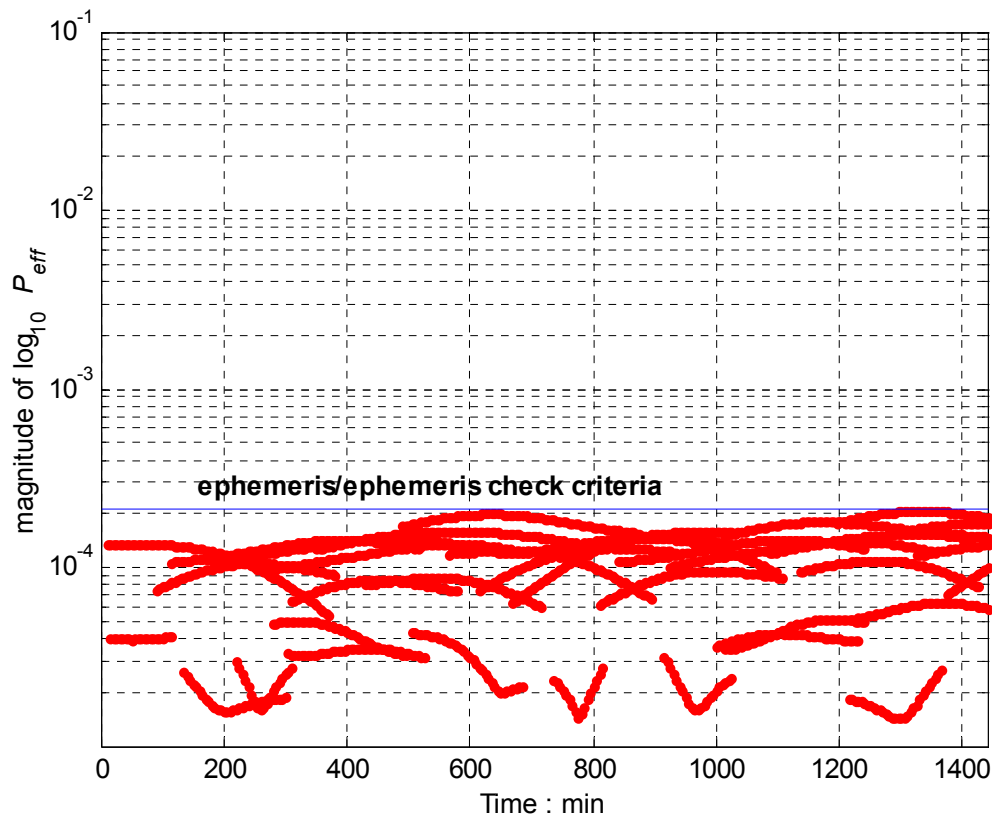


Figure 4.5 Simulation Results of P_{eff} Values by Combination Measurements

The performance of the combinational residual method may be improved further by increasing the length of the baselines. From Equation (4-18), it is obvious that the P_{eff}

value can be reduced by increasing baseline length b . In Figure 4.6, the results with 200 m baseline length clearly show improved performance.

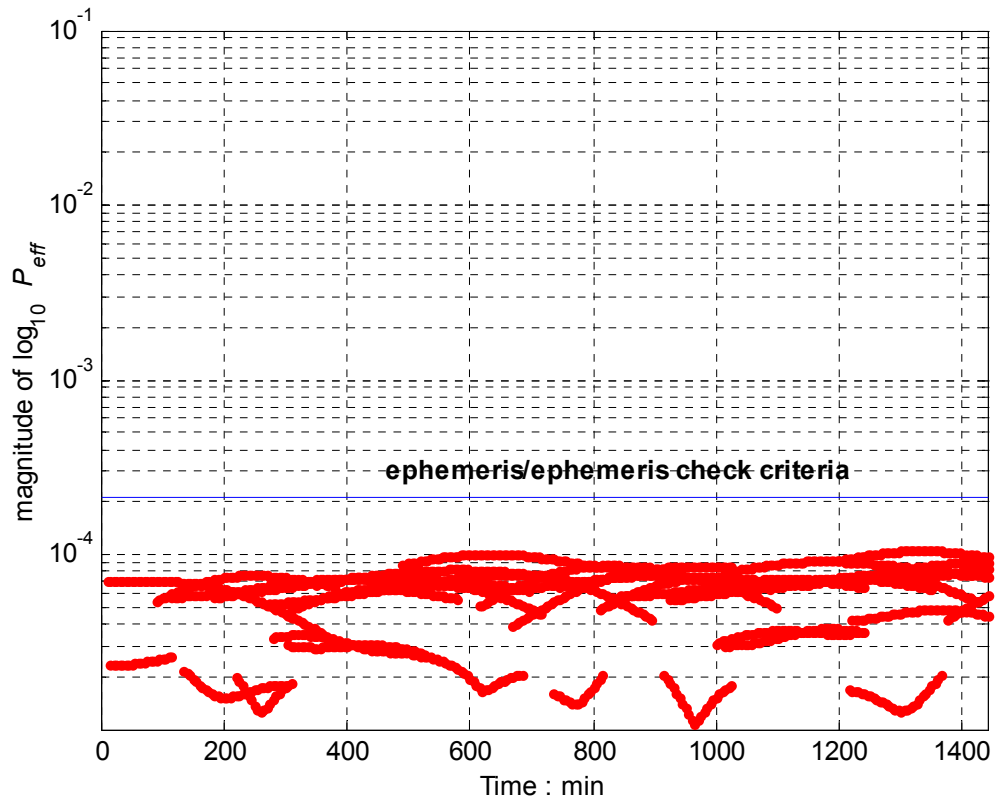


Figure 4.6 P_{eff} Values Performance Improvement by Using 200m Baseline

CHAPTER V

CONCLUSION

Differential GPS has been proven to achieve great improvement in position accuracy relative to standard GPS position. Therefore, this technique has been used widely in various applications, including the FAA's LAAS precision approach and landing system. For the LAAS application, however, navigation integrity is of equal importance to accuracy.

Correct satellite ephemeris data is fundamental to differential positioning. Therefore ephemeris monitoring is necessary to ensure navigation integrity. Although no satellite orbit errors large enough to produce significant DGPS errors have been confirmed to date, such occurrences cannot be ruled out.

For DGPS users, the components of satellite orbit error perpendicular to the satellite line-of-sight direction are of primary concern. The magnitude of effective ranging error is proportional to the distance between reference and user receivers. Therefore, the potential safety risk will increase greatly to the user requiring high accuracy and integrity at large distances from reference receiver.

The basic built-in ephemeris monitoring methods for LAAS are ephemeris/ephemeris check and MFRT. Additional proposed ephemeris integrity monitoring approaches include RAIM and DPR/DPDAS. Because the limitations of these methods, a new ephemeris monitoring algorithm is proposed to meet LAAS system performance requirements.

A new dual-frequency carrier-phase architecture to detect orbit errors affecting

LAAS user integrity was proposed in Chapters II and III. The satellite-geometry-free widelane method is used in this orbit error detection architecture to resolve the unknown cycle ambiguities in the carrier-phase measurements. Once the integers are estimated correctly, ephemeris error can be detected in real time by short baseline LGF measurements. The proposed ephemeris integrity monitoring architecture is capable of detecting both Type A and Type B ephemeris failures with reference receiver baselines of approximately 400 meters. In addition, several single frequency monitoring approaches were explored and have shown enough promise for further development, in particular for the detection of Type B failures.

APPENDIX

A. Derivation of Analytic Approach for $\delta\bar{e}_a$

Assume the nominal orbit position of satellite i , which is expressed in east-north-up local coordinates with receiver antenna a as the origin, is $[x \ y \ z]^T$. The orbit error $\delta\bar{R}_i$ is defined as $[\delta x \ \delta y \ \delta z]^T$. The range r is equal to $\sqrt{x^2 + y^2 + z^2}$. The line-of-sight unit vector can then be denoted as:

$$\bar{e}_a = \begin{bmatrix} \frac{x}{r} & \frac{y}{r} & \frac{z}{r} \end{bmatrix}^T \quad (2-6.2)$$

Taking variations on both sides of Equation (2-6.2), we have:

$$\delta\bar{e}_a = \begin{bmatrix} \delta\left(\frac{x}{r}\right) & \delta\left(\frac{y}{r}\right) & \delta\left(\frac{z}{r}\right) \end{bmatrix}^T \quad (2-6.3)$$

Expanding $\delta\left(\frac{x}{r}\right)$ gives:

$$\begin{aligned} \delta\left(\frac{x}{r}\right) &= \delta x \frac{1}{r} + x \delta\left(\frac{1}{\sqrt{x^2 + y^2 + z^2}}\right)^{-1} \\ &= \delta x \frac{1}{r} - \frac{1}{2} x \sqrt{x^2 + y^2 + z^2}^{-\frac{3}{2}} (2x\delta x + 2y\delta y + 2z\delta z) \\ &= \frac{1}{r} \delta x - \frac{x^2}{r^3} \delta x - \frac{xy}{r^3} \delta y - \frac{xz}{r^3} \delta z \\ &= \frac{1}{r} \left[\left(1 - \frac{x^2}{r^2}\right) \delta x - \frac{xy}{r^2} \delta y - \frac{xz}{r^2} \delta z \right] \\ &= \frac{1}{r} \left[(1 - \bar{e}_a^T \bar{e}_a) \delta x - \bar{e}_a^T \bar{e}_a \delta y - \bar{e}_a^T \bar{e}_a \delta z \right] \end{aligned} \quad (2-6.4)$$

where ${}_x\bar{e}_a$, ${}_y\bar{e}_a$, and ${}_z\bar{e}_a$ are the corresponding east, north, and up components of \bar{e}_a .

Similarly, one can obtain $\delta\left(\frac{y}{r}\right)$ and $\delta\left(\frac{z}{r}\right)$ as follows:

$$\delta\left(\frac{y}{r}\right) = \frac{1}{r} [{}_y\bar{e}_a^T {}_x\bar{e}_a \delta x - (1 - {}_y\bar{e}_a^T {}_y\bar{e}_a) \delta y - {}_y\bar{e}_a^T {}_z\bar{e}_a \delta z] \quad (2-6.5)$$

$$\delta\left(\frac{z}{r}\right) = \frac{1}{r} [{}_z\bar{e}_a^T {}_x\bar{e}_a \delta x - {}_z\bar{e}_a^T {}_y\bar{e}_a \delta y - (1 - {}_z\bar{e}_a^T {}_z\bar{e}_a) \delta z] \quad (2-6.6)$$

Substituting Equations (2-6.4), (2-6.5), and (2-6.6) back into Equation (2-6.3), a more concise result can be found as follows:

$$\begin{aligned} \delta\bar{e}_a &= \frac{1}{r} \begin{bmatrix} (1 - {}_x\bar{e}_a^T {}_x\bar{e}_a) \delta x - {}_x\bar{e}_a^T {}_y\bar{e}_a \delta y - {}_x\bar{e}_a^T {}_z\bar{e}_a \delta z \\ -{}_y\bar{e}_a^T {}_x\bar{e}_a \delta x + (1 - {}_y\bar{e}_a^T {}_y\bar{e}_a) \delta y - {}_y\bar{e}_a^T {}_z\bar{e}_a \delta z \\ -{}_z\bar{e}_a^T {}_x\bar{e}_a \delta x - {}_z\bar{e}_a^T {}_y\bar{e}_a \delta y + (1 - {}_z\bar{e}_a^T {}_z\bar{e}_a) \delta z \end{bmatrix} \\ &= \frac{1}{r} \begin{bmatrix} (1 - {}_x\bar{e}_a^T {}_x\bar{e}_a) & -{}_x\bar{e}_a^T {}_y\bar{e}_a & -{}_x\bar{e}_a^T {}_z\bar{e}_a \\ -{}_y\bar{e}_a^T {}_x\bar{e}_a & (1 - {}_y\bar{e}_a^T {}_y\bar{e}_a) & -{}_y\bar{e}_a^T {}_z\bar{e}_a \\ -{}_z\bar{e}_a^T {}_x\bar{e}_a & -{}_z\bar{e}_a^T {}_y\bar{e}_a & (1 - {}_z\bar{e}_a^T {}_z\bar{e}_a) \end{bmatrix} \begin{bmatrix} \delta x \\ \delta y \\ \delta z \end{bmatrix} \\ &= \frac{1}{r} \left(I - \begin{bmatrix} {}_x\bar{e}_a^T {}_x\bar{e}_a & {}_x\bar{e}_a^T {}_y\bar{e}_a & {}_x\bar{e}_a^T {}_z\bar{e}_a \\ {}_y\bar{e}_a^T {}_x\bar{e}_a & {}_y\bar{e}_a^T {}_y\bar{e}_a & {}_y\bar{e}_a^T {}_z\bar{e}_a \\ {}_z\bar{e}_a^T {}_x\bar{e}_a & {}_z\bar{e}_a^T {}_y\bar{e}_a & {}_z\bar{e}_a^T {}_z\bar{e}_a \end{bmatrix} \right) \begin{bmatrix} \delta x \\ \delta y \\ \delta z \end{bmatrix} \\ \delta\bar{e}_a &= \frac{1}{r} (\bar{I} - \bar{e}_a \bar{e}_a^T) \delta \bar{R}_i \end{aligned} \quad (2-6.7)$$

which is the same as Equation (2-6.1).

$$\begin{aligned} \delta\bar{e}_a &= \frac{1}{R_a^i - \delta \bar{R}_i \cdot \bar{e}_a} (\bar{I} - \bar{e}_a \bar{e}_a^T) \delta \bar{R}_i \\ &= \frac{1}{R_a^i \left(1 - \frac{\delta \bar{R}_i \cdot \bar{e}_a}{R_a^i}\right)} (\bar{I} - \bar{e}_a \bar{e}_a^T) \delta \bar{R}_i \end{aligned}$$

$$\begin{aligned}
&= \frac{1}{R_a^i} (\bar{I} - \bar{e}_a \bar{e}_a^T) \delta \bar{R}_i \frac{1}{(1 - \frac{\delta \bar{R}_i \cdot \bar{e}_a}{R_a^i})} \\
&= \frac{1}{R_a^i} (\bar{I} - \bar{e}_a \bar{e}_a^T) \delta \bar{R}_i [1 + \frac{\delta \bar{R}_i \cdot \bar{e}_a}{R_a^i} + (\frac{\delta \bar{R}_i \cdot \bar{e}_a}{R_a^i})^2 + \dots]
\end{aligned}$$

Neglecting 2nd and higher order terms involving $\delta \bar{R}_i$, the result is:

$$\delta \bar{e}_a = \frac{1}{R_a^i} (\bar{I} - \bar{e}_a \bar{e}_a^T) \delta \bar{R}_i$$

which is the same as Equation (2-6).

BIBLIOGRAPHY

- [Axelrad94] Axelrad, P., and Brown, R.G., "GPS Navigation Algorithm," Global Positioning System: Theory and Applications, Vol. I, pp. 409-433, AIAA, 1994.
- [AC84] Federal Aviation Administration, "Criteria for Approval of Category III Landing Weather Minima," Advisory Circular 120-28C, Washington, DC, Mar. 1984.
- [Bate71] Bate, R.R., Mueller, D.D., and White, J.E., Fundamentals of Astrodynamics, Dover Publications, Inc., 1971.
- [Brown88] Brown, R.G., and McBurney, P.W., "Self-Contained GPS Integrity Check Using Maximum Solution Separation," Journal of the Institute of Navigation, Vol. 35, No. 1, Spring 1988.
- [Brown92] Brown, R.G., "A Baseline RAIM Scheme and a Note on the Equivalence of Three RAIM Methods," Journal of the Institute of Navigation, Vol. 39, No. 3, Fall 1992.
- [Bowen86] Bowen, R., "GPS Control System Accuracies," Global Positioning System, Vol. III, pp. 250, Institute of Navigation, 1986.
- [Davis93] Davis, J.M., and Kelly, R.J., "RNP Tunnel Concept for Precision Approach with GNSS Application," Proceedings of Institute of Navigation 49th Annual Meeting, Cambridge, MA, June 1993.
- [GPSSPS] Global Positioning System Standard Positioning Service Signal Specification, 2nd Edition, Jun. 1995. Internet sit: <http://www.navcen.uscg.gov/pubs/sigspec/>,
- [Gelb74] Gelb, A., Kasper Jr., J.F., Nash Jr., R.A., Price, C.F., and Sutherland Jr., A.A., Applied Optimal Estimation, M.I.T. Press, 1974.
- [Heo00] Heo, M., "Study of Carrier phase measurement Error by Satellite Elevation Angle," IIT Research Briefing,
- [ICD-200] Interface Control Document (ICD) GPS-200, Revision B, Rockwell International, 1987.
- [Kaplan76] Kaplan, M.H., Modern Spacecraft Dynamics & Control, John Wiley & Sons. Inc., 1976.
- [Keyton90] Kayton, M., Navigation: Land, Sea, Air and Space, IEEE Press, New York, 1990

- [Liu97] Liu, F., Murphy, T., and Skidmore, T.A., "LAAS Signal-in-Space Integrity Monitoring Description and Verification Plan," Proceedings of the 10th International Meeting of the Satellite Division of the Institute of Navigation, city, state, 1997.
- [Misra99] Misra, P., Burke, B.P., and Pratt, M.M., "GPS Performance in Navigation," Transactions of the IEEE. VOL.87, No.1, Jan. 1999.
- [Matsu97] Matsumoto, S., Pullen, S., Rotkowitz, M. and Pervan, B.S., "GPS Ephemeris Verification for Local Area Augmentation System (LAAS) Ground Stations," Proceedings of the 10th International Meeting of the Satellite Division of the Institute of Navigation, Nashville, TN, 1999.
- [MASPS98] "Minimum Aviation System Performance Standards for The Local Area Augmentation System," RTCA Paper No. 037-98/SC159-778, Feb. 1998.
- [ORD95] Operational Requirements Document, "Local Area Augmentation System," Satellite Navigation Program Office, Federal Aviation Administration, Feb. 1995.
- [Parkin94] Parkinson, B., "Introduction and Heritage of NAVSTAR, the Global Positioning System," Global Positioning System: Theory and Applications, Vol. I, pp. 3-28, AIAA, 1994.
- [Parkin88] Parkinson, B., and Axelrad P., "Autonomous Integrity Monitoring Using the Pseudorange Residual," Journal of the Institute of Navigation, Vol. 35, No. 2, Summer 1988..
- [Parkin95] Parkinson, B., and Enge, P.K., "Differential GPS," Global Positioning System: Theory and Applications, Vol. II, pp. 3-50, AIAA, 1995.
- [Pervan96] Pervan, B., "Navigation Integrity for Aircraft Precision Landing Using The Global Positioning System," Stanford University Ph.D. Dissertation, Department of Aeronautics and Astronautics, Mar. 1996.
- [PT1LAAS] "Specification: Performance Type One Local Area Augmentation System Ground Facility," United States Department of Transportation, Federal Aviation Administration, FAA-E-2937, Sep. 1999.
- [Rivers00] Rivers, M.H., "2 SOPS Anomaly Resolution on an Aging Constellation." ION GPS-2000, Sep. 2000.
- [Shively01] Shively, C.A., "Preliminary Analysis of Requirements for Cat IIIB LAAS," Proceedings of the 57th Annual Meeting of the Institute of Navigation, Albuquerque, NM, Jun. 2001.

- [Spilker94a] Spilker Jr., J.J., "GPS Navigation Data," Global Positioning System: Theory and Applications, Vol. I, pp. 121-176, AIAA, 1994.
- [Spilker94b] Spilker Jr., J.J., "Satellite Constellation and Geometric Dilution of Precision," Global Positioning System: Theory and Applications, Vol. I, pp. 177-208, AIAA, 1994.
- [Spilker94c] Spilker Jr., J.J., and Parkinson, B.W., "Overview of GPS Operation and Design," Global Positioning System: Theory and Applications, Vol. I, pp. 29-55, AIAA, 1994.
- [Sturza88] Sturza, M.A., "Navigation System Integrity Monitoring Using Redundant Measurements," Journal of the Institute of Navigation, Vol. 35, No. 4, Winter 1988-89.
- [WGS84] Anon., "Department of Defense World Geodetic System, 1984(WGS84), Its definition and Relationships with Local Geodetic System," DMA-TR-8350.2, Defense Mapping Agent (DMA), Sep. 1987.
- [Walter95] Walter, T., and Enge, P., "Weighted RAIM for Precision Approach," Proceedings of the 6th International Meeting of the Satellite Division of the Institute of Navigation, Palm Spring, CA, Sep. 1995.
- [Warb99] Warburton, J., Lamb, D., "Validation of the FAA LAAS Specification Using the LAAS Test Prototype (LTP)," Journal of the Institute of Navigation, Vol. 45, No. 4, Winter 1998-99.